Production of energetic light fragments in extensions of the CEM and LAQGSM event generators of the Monte Carlo transport code MCNP6

Stepan G. Mashnik,[1,*] Leslie M. Kerby,[1,2,3,†] Konstantin K. Gudima,[4] Arnold J. Sierk,[1,‡]
Jeffrey S. Bull,[1] and Michael R. James[1]

[1]*Los Alamos National Laboratory, Los Alamos, New Mexico 87545, USA*
[2]*Idaho State University, Pocatello, Idaho 83201, USA*
[3]*Idaho National Laboratory, Idaho Falls, Idaho 83402, USA*
[4]*Institute of Applied Physics, Academy of Science of Moldova, Chişinău, Moldova*

(Received 12 July 2016; published 23 March 2017)

We extend the cascade-exciton model (CEM), and the Los Alamos version of the quark-gluon string model (LAQGSM), event generators of the Monte Carlo N-particle transport code version 6 (MCNP6), to describe production of energetic light fragments (LF) heavier than ^{4}He from various nuclear reactions induced by particles and nuclei at energies up to about 1 TeV/nucleon. In these models, energetic LF can be produced via Fermi breakup, preequilibrium emission, and coalescence of cascade particles. Initially, we study several variations of the Fermi breakup model and choose the best option for these models. Then, we extend the modified exciton model (MEM) used by these codes to account for a possibility of multiple emission of up to 66 types of particles and LF (up to ^{28}Mg) at the preequilibrium stage of reactions. Then, we expand the coalescence model to allow coalescence of LF from nucleons emitted at the intranuclear cascade stage of reactions and from lighter clusters, up to fragments with mass numbers $A \leqslant 7$, in the case of CEM, and $A \leqslant 12$, in the case of LAQGSM. Next, we modify MCNP6 to allow calculating and outputting spectra of LF and heavier products with arbitrary mass and charge numbers. The improved version of CEM is implemented into MCNP6. Finally, we test the improved versions of CEM, LAQGSM, and MCNP6 on a variety of measured nuclear reactions. The modified codes give an improved description of energetic LF from particle- and nucleus-induced reactions; showing a good agreement with a variety of available experimental data. They have an improved predictive power compared to the previous versions and can be used as reliable tools in simulating applications involving such types of reactions.

DOI: 10.1103/PhysRevC.95.034613

I. INTRODUCTION

The Los Alamos National Laboratory (LANL) Monte Carlo N-particle transport code MCNP6 [1] uses by default the latest version of the cascade-exciton model (CEM), CEM03.03 [2–4], as its event generator to simulate reactions induced by nucleons, pions, and photons of energies up to 4.5 GeV and the Los Alamos version of the quark-gluon string model (LAQGSM), LAQGSM03.03 [4–6], to simulate such reactions at higher energies, as well as reactions induced by other elementary particles and by nuclei of all energies up to ∼1 TeV/nucleon.

MCNP6 is used around the world by several thousands of users in applications ranging from radiation protection and dosimetry, nuclear-reactor design, nuclear criticality safety, detector design and analysis, decontamination and decommissioning, accelerator applications, medical physics, space research, and beyond. This is why it is important that MCNP6 predicts as well as possible arbitrary nuclear reactions, including production of energetic light fragments (LF).

At lower energies, MCNP6 uses tables of evaluated nuclear data (referred to as "data libraries"), while for higher energies (>150 MeV), MCNP6 uses CEM03.03 and LAQGSM03.03 as mentioned above, as well as by default for some reactions, or when chosen by users, the Bertini intranuclear cascade (INC) [7], ISABEL [8], or the INC developed at Liege (INCL) by Cugnon and colleagues from CEA/Saclay, France, version INCL4.2 [9], merged with the evaporation/fission and Fermi breakup models available in MCNP6 (see details in Ref. [1]).

Emission of energetic heavy clusters from nuclear reactions plays a critical role in several applications, including electronics performance in space, human radiation dosages in space or other extreme radiation environments, proton and heavy-ion therapy in cancer treatment, accelerator and shielding applications, and more.

Understanding the production of LF is very interesting also from a scientific point of view, as there is still uncertainty about the dependences of the different reaction mechanisms on the energy of the inducing particle, the mass number of the target, and the type and emission energy of the fragments. To the best of our knowledge, none of the currently available simulation tools are able to accurately predict emission of LF from arbitrary reactions. This research may help to understand better the mechanisms of nuclear reactions at intermediate and high energies.

This work focuses significantly on the emission of high-energy LF at the preequilibrium stage of nuclear reactions, as considered in these models. However, high-energy LF can be produced by other reaction mechanisms. For example, Cugnon *et al.* have extended their Liège intranuclear cascade (INCL) code to consider emission of LF heavier than ^{4}He during the

*Deceased.
†kerblesl@isu.edu
‡t2ajs@lanl.gov

cascade stage of reactions via coalescence of several nucleons at the nuclear periphery [10]. But INCL has not yet been generalized across all types of nuclear reactions; it does not work yet for heavy-ion-induced reactions and is currently limited to incident energies only below several GeV/nucleon The most advanced versions of INCL so far published work only for projectiles with $A \leqslant 18$ and at incident energies below 15–20 GeV/nucleon.

Emission of ^{7}Be at the preequilibrium stage (described by a hybrid exciton model and coalescence pick-up model) was studied by Konobeyev and Korovin two decades ago [11]. Preequilibrium emission of helium and lithium ions was discussed in Ref. [12]. Preequilibrium emission of light fragments was also studied within the CEM in 2002 [13], but that project was never completed.

Besides preequilibrium emission, energetic fragments can be produced also via Fermi breakup [14] and multifragmentation processes, as described, e.g., by the statistical multifragmentation model (SMM) [15].

Additionally, energetic LF could in principle also be produced at the earliest stages of nuclear reactions as described by various versions of quantum molecular dynamics (QMD) (see, e.g., Ref. [16] and references therein). With sufficient development, QMD might be able to describe fragment production of the sort considered in this paper. However, currently it does not have as good a predictive power as do simpler and much faster INC-type models. We are not aware of any publication where LF spectra are predicted well by a version of QMD. In addition, as was determined by three international comparisons of models and codes for spallation reaction applications performed since 1992 under the auspices of the Nuclear Energy Agency of the Organization for Economic Co-operation and Development (NEA/OECD) and the International Atomic Energy Agency (IAEA), generally, all tested versions of QMD showed a worse predictive power in comparison with INC-type models. In addition, current QMD codes are about 100–300 times slower than INC-type event generators, which makes them less practical for complex simulation applications, even those using currently available supercomputers. Therefore, QMD is not yet ready to be widely used in realistic nuclear simulation applications (see details and references, e.g., in Refs. [17,18]).

Lastly, the authors of most of the recent measurements of LF spectra analyze their experimental data using different simplified approaches assuming emission of LF from moving sources (see, e.g., Refs. [19–21]). Such simplified moving-source prescriptions are fitted to describe as well as possible only their own measured LF spectra, and have not been developed further to become universal models with predictive power for spectra of LF from arbitrary reactions. Such approaches cannot describe at all many other characteristics of nuclear reactions, such as the yields and energies of spallation products, fission-fragment production, etc., and therefore cannot be used as event generators in transport codes.

For detailed information on spallation reactions, models, and researches, see the book *Handbook of Spallation Research*, by Filges and Goldenbaum [17]. A useful recent summary paper by David, on spallation models, is available in Ref. [18].

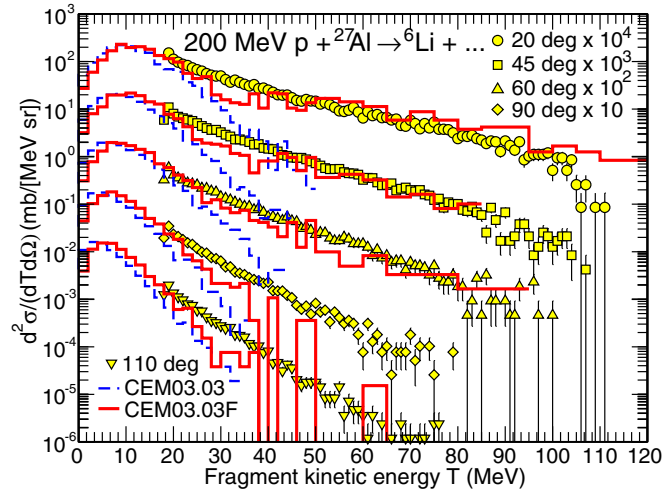

FIG. 1. Comparison of experimental ^{6}Li spectra at 20, 45, 60, 90, and 110 degrees by Machner *et al.* [19] (open symbols) with calculations by the unmodified CEM03.03 (dashed histograms) and results by the newly revised CEM03.03F (solid histograms), as discussed in the text.

The CEM and LAQGSM event generators in MCNP6 describe quite well the spectra of emitted particles and of fragments with sizes up to ^{4}He across a broad range of target masses and incident energies (up to ∼5 GeV for CEM and up to ∼1 TeV/nucleon for LAQGSM), as well as the yields of most spallation and fission products (see, e.g., Refs. [4,22,23] and references therein). However, as shown by dashed histograms in Fig. 1, these models do not predict well the high-energy tails of LF spectra heavier than ^{4}He.

This is true for other projectiles, incident energies, and target mass numbers for all fragments heavier than ^{4}He. At lower energies of ejectiles ($\lesssim$25 MeV), CEM describes well the data, but for intermediate energies ($\gtrsim$25 MeV) the CEM predictions fall off sharply. This is because the only mechanism currently included for producing ^{6}Li fragments is evaporation, which considers emission of LF (up to ^{28}Mg) [24]. At higher energies ($\gtrsim$25 MeV), the fragments should largely be produced by these models at the preequilibrium stage which would require an improved modified exciton model (MEM), as well as a contribution from the coalescence of nucleons produced in the INC with $A > 4$. Neither the MEM nor the coalescence model used by the 03.03 versions of CEM and LAQGSM considers these heavier fragments.

The aim of this work is to extend the precompound model in these event generators to include such processes, leading to an increase of predictive power for LF production in MCNP6. This entails upgrading the MEM currently used at the preequilibrium stage in CEM and LAQGSM. It also includes verifying and extending the coalescence and the Fermi breakup models used in the precompound stages of spallation reactions within CEM and LAQGSM.

II. CEM AND LAQGSM OVERVIEW

Details, examples of results, and useful references to different versions of CEM and LAQGSM may be found in a recent lecture [4].

The cascade-exciton model of nuclear reactions was proposed more than 30 years ago at the Laboratory of Theoretical Physics, JINR, Dubna, USSR by Gudima, Mashnik, and Toneev [3]. It is based on the standard (non-time-dependent) Dubna intranuclear cascade model [25,26] and the modified exciton model [27,28]. The code LAQGSM03.03 is the latest modification [6] of LAQGSM [5], which in its turn is an improvement of the quark-gluon string model (QGSM) [29]. It describes reactions induced by both particles and nuclei at incident energies up to about 1 TeV/nucleon.

The basic versions of both the CEM and LAQGSM event generators are the so-called "03.03" versions, namely CEM03.03 [2–4] and LAQGSM03.03 [4–6]. The CEM code calculates nuclear reactions induced only by nucleons, pions, and photons. It assumes that the reactions occur in three stages. The first stage is the INC, in which primary particles can be rescattered and produce secondary particles several times prior to absorption by, or escape from, the nucleus. When the cascade stage of a reaction is completed, CEM uses the coalescence model to create high-energy d, t, ^{3}He, and ^{4}He by final-state interactions among emitted cascade nucleons outside the target. The emission of the cascade particles determines the particle-hole configuration, Z, A, and the excitation energy that comprise the starting conditions for the second, preequilibrium stage of the reaction. The subsequent relaxation of the nuclear excitation is treated in terms of an improved version of the MEM of preequilibrium decay, followed by the equilibrium evaporation/fission stage described using a modification of the generalized evaporation model (GEM) code GEM2 by Furihata [24].

Generally, all three components may contribute to experimentally measured particle spectra and other distributions. But if the residual nuclei after the INC have atomic numbers with $A \leqslant A_{\rm Fermi} = 12$, CEM uses the Fermi breakup model to calculate their further disintegration instead of using the preequilibrium and evaporation models. Fermi breakup, which estimates the probabilities of various final states by calculating the approximate phase space available for each configuration, is much faster to calculate and gives results very similar to those from using the continuation of the more detailed models for lighter nuclei. LAQGSM also describes nuclear reactions as a three-stage process: an INC, followed by preequilibrium emission of particles during the deexcitation of the excited residual nuclei formed after the INC, followed by evaporation of particles from and/or fission of the compound nuclei. LAQGSM was developed with a primary focus on describing reactions induced by nuclei, as well as induced by most elementary particles, at high energies, up to about 1 TeV/nucleon. The INC of LAQGSM is completely different from that in CEM. LAQGSM also considers Fermi breakup of nuclei with $A \leqslant 12$ produced after the cascade, and the coalescence model to produce high-energy d, t, ^{3}He, and ^{4}He from nucleons emitted during the INC.

From this brief overview of these models, it is clear that energetic LF can only be produced in this approach through one of the following three processes: Fermi breakup, preequilibrium emission, and coalescence. Below, we explore each of these mechanisms.

Many people participated in the development of CEM and LAQGSM over their more than 40-year history. Contributors to the "03.03" versions are Mashnik, Gudima, Sierk, Prael, Baznat, and Mokhov. Kerby joined these efforts recently, primarily to extend the precompound models of CEM and LAQGSM by accounting for possible emission of LF heavier than ^{4}He, specifically up to ^{28}Mg.

For more details on the physics of CEM and LAQGSM, see Ref. [4] and references therein.

III. FERMI BREAKUP

Generally, after the fast INC stage of a nuclear reaction, a much slower evaporation/fission stage follows, with or without taking into account an intermediate preequilibrium stage between the INC and the equilibrated evaporation/fission. Such a picture is well grounded in the case of heavy nuclei, as both evaporation and fission models are based on statistical assumptions, requiring a large number of nucleons. Naturally, in the case of light nuclei with only a few nucleons, statistical models are less well justified. In addition, such light nuclei like carbon and oxygen exhibit considerable α-particle clustering, not accounted for in evaporation/fission models. This is why in the case of light excited nuclei, their deexcitation is often calculated using the so-called Fermi breakup model, suggested initially by Fermi [14].

It is impossible to measure all nuclear data needed for applications involving light target nuclei; therefore, Monte Carlo transport codes are usually used to simulate fragmentation reactions. It is important that available transport codes predict such reactions as well as possible. For this reason, efforts have been made recently to investigate the validity and performance of, and to improve where possible, nuclear reaction models used by such transport codes as GEANT4 (e.g., [30]), SHIELD-HIT (e.g., [31]), PHITS (e.g., [32]), as well as MCNP6 (e.g., [33,34]).

Deexcitation of light nuclei with $A \leqslant A_{\rm Fermi}$ remaining after the INC, the preequilibrium model, or at any stage of the fission/evaporation model, is described in CEM and LAQGSM only with the Fermi breakup model, where $A_{\rm Fermi}$ is a "cutoff value" fixed in the models. The value of $A_{\rm Fermi}$ is a model parameter, not a physical characteristic of nuclear reactions. Actually, the initial version of the Fermi breakup model incorporated into CEM and LAQGSM (see details in Ref. [4]) used $A \leqslant A_{\rm Fermi} = 16$, just as $A_{\rm Fermi} = 16$ is used currently in GEANT4 (see [30]) and in SHIELD-HIT (see [31]). But that initial version of the Fermi breakup model had some problems and caused code crashes in some cases (see details in Ref. [4]). To avoid unphysical results and code crashes, we chose the expedient of using $A_{\rm Fermi} = 12$ in both CEM and LAQGSM. Later, the problems in the Fermi breakup model were fixed in the codes, but the value of $A_{\rm Fermi}$ was not changed. We now address how its value affects the results of these codes, calculating spectra of emitted particles and LF, and yields of all possible products from various reactions using different values for $A_{\rm Fermi}$.

One of the most difficult tasks for any theoretical model is to predict cross sections of arbitrary products as functions of the incident energy of the projectile initiating the reaction,

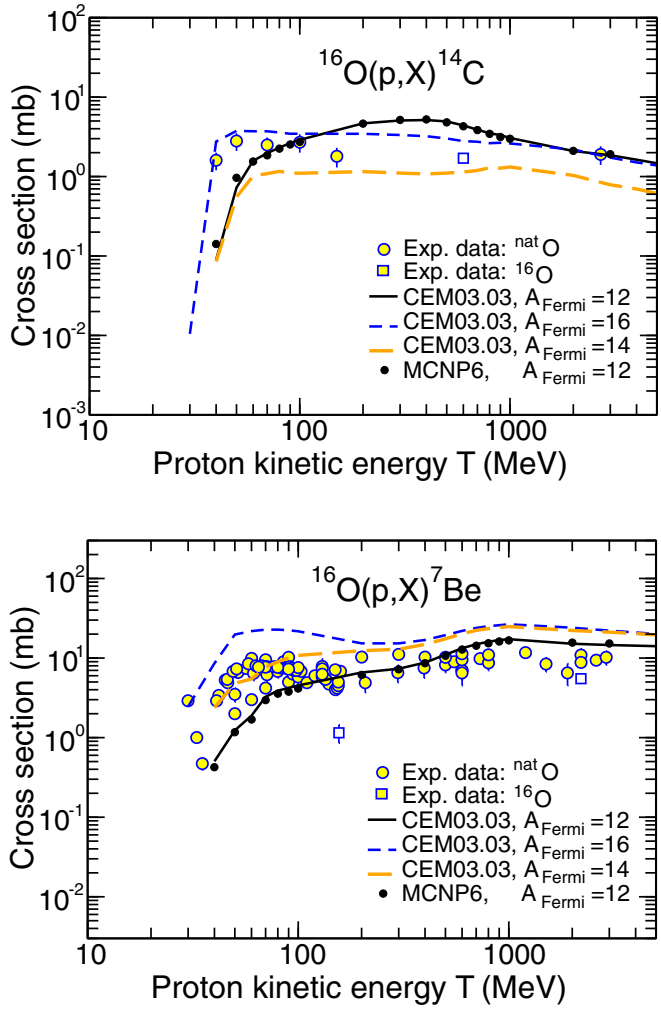

FIG. 2. Excitation functions for the production of ^{14}C and ^{7}Be, calculated with CEM03.03 using the "standard" version of the Fermi breakup model ($A_{Fermi} = 12$) and with cutoff values A_{Fermi} of 14 and 16 (lines), as well as with MCNP6 using CEM03.03 ($A_{Fermi} = 12$; solid points) compared with experimental data (open symbols), as indicated. Experimental data are from the T16 Lib compilation [35].

i.e., "excitation functions." Therefore, we start the study by comparing the available experimental data on excitation functions of products from several proton-induced reactions on light nuclei at intermediate energies with predictions by MCNP6 using its default event generator for such reactions, CEM03.03, as well as with results calculated by CEM03.03 used as a stand-alone code.

We show as examples two excitation functions, for proton-induced reactions on ^{16}O. Many more results can be found in Ref. [33]. Figure 2 presents results for the reaction $p + {}^{16}$O. Most of the experimental data for these reactions were measured on ^{nat}O targets, with only a few data points obtained for pure ^{16}O; all the calculations use ^{16}O. For these reactions, we perform three sets of calculations, using $A_{Fermi} = 12$, 14, and 16 in CEM03.03. The general agreement/disagreement of the results with available measured data for oxygen is very similar to what was displayed in Ref. [33] for $p + {}^{14}$N, ^{27}Al, or ^{nat}Si.

Our results demonstrate very good agreement between the excitation functions simulated by MCNP6 using CEM03.03 and calculations by the stand-alone CEM03.03, and a reasonable agreement with most of the available experimental data. This serves as a validation of MCNP6 and demonstrates there are no problems with the incorporation of CEM03.03 into MCNP6 or with the simulations of these reactions by either code.

The observed discrepancies between some calculated excitation functions and measured data at energies below 20 MeV are not of concern for our current emphasis. As a default, MCNP6 uses data libraries at such low energies and never uses CEM03.03 or other event generators, when data libraries are available, as is the case for the reactions studied here. By contrast, CEM uses its INC to simulate the first stage of nuclear reactions, and the INC is not expected to work properly at such low energies (see details in Refs. [2,4]).

Results calculated with the values of $A_{Fermi} = 12$, 14, and 16 all agree reasonably well with available data, taking into account that all calculations, at all energies and for all reactions, are done with the default versions of these codes, without varying any parameters. However, in some cases, there are significant differences between excitation functions calculated with $A_{Fermi} = 12$ and 16.

For many cases, a better description of the heavier fragments occurs for $A_{Fermi} = 16$ or 14, and usually the LF are better described using $A_{Fermi} = 12$. However, the model with any of these values agrees reasonably well with the measured data, especially for LF with $Z \leqslant 4$ (e.g., [33]). For LF with $Z > 4$, it is difficult to determine which value agrees better with the data: $A_{Fermi} = 12$ or $A_{Fermi} = 16$. Light fragments with $Z = 3$ and 4 are described a little better with $A_{Fermi} = 12$. As discussed below, preequilibrium emission described with an extended version of the MEM (not accounted for in the calculations shown in Fig. 2), can be important and may change the final CEM results for such reactions; therefore, we do not make yet a final decision about which value of the Fermi breakup cutoff works better, keeping the previous value of 12 until a more careful analysis can be performed.

After analyzing all excitation functions for the light targets where Fermi breakup dominates, for which we found reliable experimental data, we then study spectra of particles and LF from proton-induced reactions on light nuclei, where the Fermi breakup mechanism should manifest itself most clearly. We show only two examples of double differential spectra. Many more examples are presented in Ref. [33], some of which address different reaction mechanisms for fragment production, with some involving more than one mechanism in the production of the same LF in a given reaction.

Figure 3 shows examples of measured ^{6}Li and ^{7}Be spectra from $p + {}^{9}$Be at 190 MeV [36], compared to CEM results. Because ^{9}Be has a mass number $A < A_{Fermi} = 12$, all the LF from these reactions are calculated either as fragments from the Fermi breakup of the excited nuclei remaining after the initial INC stage, or as residual nuclei after emission of several particles from the ^{9}Be target nucleus during the INC. No preequilibrium or evaporation mechanisms are considered. There is a reasonably good agreement of the CEM predictions with the measured spectra from all reactions we tested, at

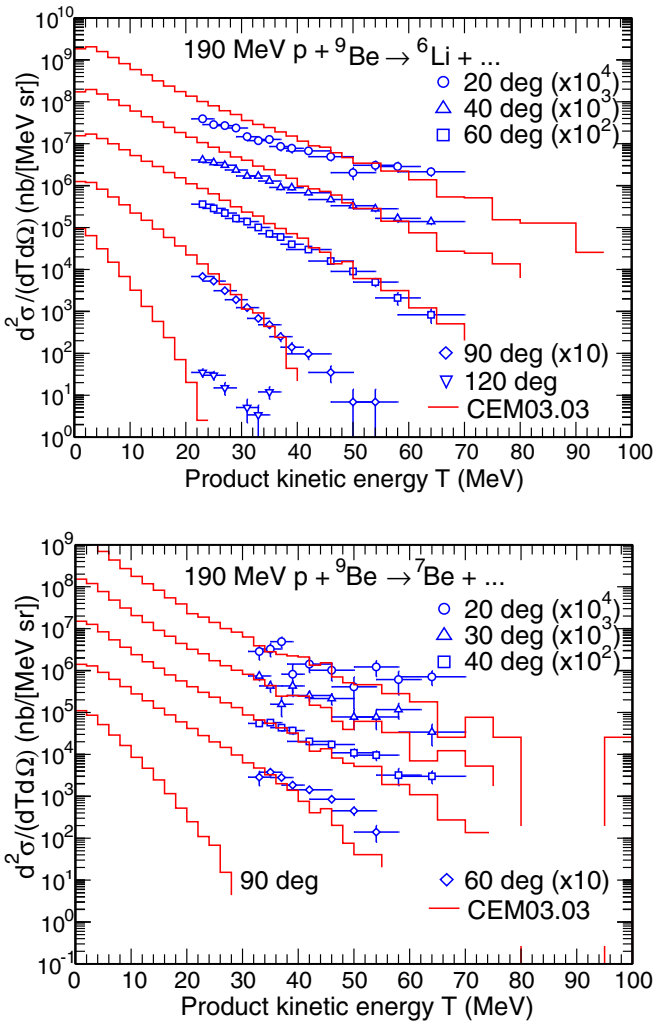

FIG. 3. Examples of measured ^{6}Li and ^{7}Be double-differential spectra from $p + {}^{9}$Be at 190 MeV [36] (open symbols), compared to CEM results (histograms).

different incident energies, from different light target nuclei, and for all products where we found experimental data: protons, complex particles, and LF heavier than ^{4}He (see examples of more results and details in Ref. [33]).

As a particular case, we test how well the Fermi breakup model used in these codes describes so-called "limiting fragmentation" reactions. The limiting fragmentation hypothesis, first proposed by Benecke *et al.* [37], suggests that fragmentation cross sections reach asymptotic values at sufficiently high incident-projectile energies. In other words, above a given bombarding energy, both the differential and total production cross sections remain constant. Figure 4 illustrates the validity of the limiting fragmentation hypothesis for the ^{4}He spectra at 35 degrees from 1.2, 1.9, and 2.5 GeV $p + {}^{12}$C reactions measured by Fidelus of the PISA Collaboration [38].

In Refs. [39,40], we show similar results calculated by MCNP6 using CEM03.03, as well as a comparison of MCNP6 results with the yields (total production cross sections) of all measured fragments, from protons to ^{12}N, from the same reactions.

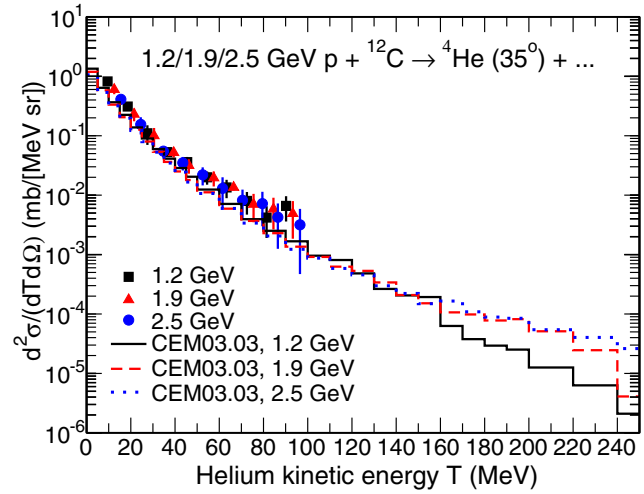

FIG. 4. ^{4}He spectra at 35° for 1.2, 1.9, and 2.5 GeV $p + {}^{12}$C measured by Fidelus of the PISA Collaboration [38] (solid symbols) compared to calculations by CEM03.03 (histograms).

We conclude that the limiting fragmentation hypothesis is supported by measurements for $p + {}^{12}$C interactions, and predicted by these models, in which the Fermi breakup mechanism plays a major role.

An independent test of the Fermi breakup model used in CEM03.03 and LAQGSM03.03 was performed recently by Konobeyev and Fischer [41] for the Fall 2014 Nuclear Data Week. These authors calculated with MCNP6 using its Bertini [7], ISABEL [8], INCL4.2+ABLA [9,42], and CEM03.03 event generators [2], as well as with the TALYS code [43]; all the experimental spectra of ^{3}He and ^{4}He measured in Ref. [36] from the reaction 190 MeV $p + {}^{9}$Be; all spectra of p, d, t, ^{3}He, and ^{4}He from the reaction of 300 MeV $p + {}^{9}$Be [36]; as well as all neutron spectra from interactions of 113 MeV protons with ^{9}Be [44] and from 256 MeV $p + {}^{9}$Be [45]. As is often done in the literature, to get quantitative estimates of the degree of fidelity to data of the spectra calculated by different models, the authors performed a detailed statistical analysis using nine different "deviation factors," namely, H, R^{CE}, R^{EC}, $\langle F \rangle$, S, L, $P_{2.0}$, $P_{10.0}$, and N_x. The definition of each can be found in Ref. [41]. The authors found that results by CEM03.03 for these particular reactions agree better with the experimental data than all the other models tested. As ^{9}Be has a mass number of 9, all these reactions are calculated using the INC followed by the Fermi breakup model. The better results from CEM03.03 in comparison to the other models prove that the Fermi breakup model used by CEM03.03 and LAQGSM03.03 in MCNP6 is reliable and can be used with confidence as a good predictive tool for various nuclear applications and academic studies.

IV. EXTENDING THE PREEQUILIBRIUM MODEL

The preequilibrium interaction stage of nuclear reactions is considered by the current CEM and LAQGSM codes in the framework of the latest version of the MEM [27,28], as described in Refs. [2,4]. At the preequilibrium stage of a

reaction, CEM03.03 and LAQGSM03.03 take into account all possible nuclear transitions changing the number of excitons n with $\Delta n = +2, -2$, and 0, as well as all possible multiple subsequent emissions of n, p, d, t, ^{3}He, and ^{4}He. The corresponding system of master equations describing the behavior of a nucleus at the preequilibrium stage is solved by the Monte Carlo technique [3]. In this section, we extend the MEM to include the possibility of emitting heavy clusters, with $A > 4$, up to ^{28}Mg.

The probability of finding the nuclear system at time t in the $E\alpha$ state, $P(E,\alpha,t)$, is describe in MEM by the differential equation

$$\frac{\delta P(E,\alpha,t)}{\delta t} = \sum_{\alpha' \neq \alpha} [\lambda(E\alpha, E\alpha')P(E,\alpha',t) - \lambda(E\alpha', E\alpha)P(E,\alpha,t)]. \quad (1)$$

Here $\lambda(E\alpha, E\alpha')$ is the energy-conserving probability rate, defined in the first-order of the time-dependent perturbation theory as

$$\lambda(E\alpha, E\alpha') = \frac{2\pi}{\hbar} |\langle E\alpha | V | E\alpha' \rangle|^2 \omega_\alpha(E), \quad (2)$$

where $\hbar$ is Planck's constant divided by 2π. The matrix element $\langle E\alpha | V | E\alpha' \rangle$ is believed to be a smooth function of energy, and $\omega_\alpha(E)$ is the density of the final states of the system. We note that Eq. (1) is derived assuming that the memory time $\tau_{\rm mem}$ of the system is small compared to the characteristic time for intranuclear transitions $\hbar/\lambda(E\alpha, E\alpha')$ but, on the other hand, Eq. (1) itself is applicable for times $t \gg \hbar/\lambda(E\alpha, E\alpha')$. Due to the condition $\tau_{\rm mem} \ll \hbar/\lambda(E\alpha, E\alpha')$, being described by Eq. (1), the random process is a Markovian one.

The MEM [27,28] utilized by CEM and LAQGSM uses effectively the relationship of the master equation (1) with Markovian random processes. Indeed, the attainment of statistical equilibration described by Eq. (1) is an example of a discontinuous Markovian process: the temporal variable changes continuously and at a random moment the state of the system changes by a discontinuous jump, the behavior of the system at the next moment being completely defined by its present state. As long as the transition probabilities $\lambda(E\alpha, E\alpha')$ are time independent, the waiting time for the system in the $E\alpha$ state has an exponential distribution (Poisson flow) with the average lifetime $\hbar/\Lambda(\alpha, E) = \hbar/\sum_{\alpha'} \lambda(E\alpha, E\alpha')$. This prompts a simple method of solving the related system of Eq. (1): simulation of the random process by the Monte Carlo technique. In this treatment, it is possible to generalize the exciton model to all nuclear transitions with $\Delta n = 0, \pm 2$, and the multiple emission of particles and to depletion of nuclear states due to particle emission. In this case the system (1) becomes [3]

$$\begin{aligned}\frac{\delta P(E,\alpha,t)}{\delta t} &= -\Lambda(n,E)P(E,n,t) \\ &\quad + \lambda_+(n-2,E)P(E,n-2,t) \\ &\quad + \lambda_0(n,E)P(E,n,t) \\ &\quad + \lambda_-(n+2,E)P(E,n+2,t) \\ &\quad + \sum_j \int dT \int dE' \lambda_j(n,E,T) \\ &\quad \times P(E',n+n_j,t)\delta(E'-E-B_j-T). \quad (3)\end{aligned}$$

For this form of the master equation (3), we need the particle emission rates λ_j and the exciton transition rates λ_+, λ_0, and λ_-.

According to the detailed-balance principle, the emission width Γ_j, can be estimated as [3]

$$\Gamma_j(p,h,E) = \int_{V_j^c}^{E-B_j} \lambda_j(p,h,E,T)dT, \quad (4)$$

where the partial transmission probabilities, λ_j, are equal to

$$\begin{aligned}\lambda_j(p,h,E,T) &= \frac{2s_j+1}{\pi^2\hbar^3}\mu_j \frac{\omega(p-1,h,E-B_j-T)}{\omega(p,h,E)} \\ &\quad \times \Re(p,h)T\sigma_j^{\rm inv}(T), \quad (5)\end{aligned}$$

where p, h, E, and ω are the number of particle excitons, the number of hole excitons, the excitation energy of the excited nucleus, and the level density of its n-exciton state, while s_j, B_j, V_j^c, μ_j, T, and $\sigma_j^{\rm inv}$ are the spin, the binding energy, the Coulomb barrier, the reduced mass, the kinetic energy, and the inverse cross section of the emitted particle j, respectively. The factor $\Re_j(p,h)$ ensures the condition for the exciton chosen to be the particle of type j and can easily be calculated by the Monte Carlo technique.

Equation (5) describes the emission of neutrons and protons only (an extension of Eq. (5) for the case of complex particles can be found in Ref. [3]). For complex particles, the level density formula ω becomes more complicated and an extra factor γ_j must be introduced (e.g., [3]):

$$\gamma_j \approx p_j^3 \left(\frac{p_j}{A}\right)^{p_j-1}. \quad (6)$$

Equation (6) for γ_j is actually only a rough estimation that is refined in CEM03.03 by parameterizing it over a mesh of residual nuclear energy and mass number (see e.g., [2]).

Assuming an equidistant level scheme with the single-particle density g, the level density of the n-exciton state is [46]

$$\omega(p,h,E) = \frac{g(gE)^{p+h-1}}{p!h!(p+h-1)!}. \quad (7)$$

This expression should be substituted into Eq. (5) to obtain the transmission rates λ_j.

According to Eq. (2), for a preequilibrium nucleus with excitation energy E and number of excitons $n = p + h$, the partial transition probabilities changing the exciton number by Δn are

$$\lambda_{\Delta n}(p,h,E) = \frac{2\pi}{\hbar} |M_{\Delta n}|^2 \omega_{\Delta n}(p,h,E). \quad (8)$$

For these transition rates, one needs the number of states, ω, taking into account the selection rules for intranuclear exciton-exciton scattering. The appropriate formulas have been derived by Williams [47] and later corrected for the exclusion principle

and indistinguishability of identical excitons in Refs. [48,49]:

$$\begin{aligned}\omega_+(p,h,E) &= \frac{1}{2}g\frac{[gE-\mathcal{A}(p+1,h+1)]^2}{n+1}\\ &\quad\times\left[\frac{gE-\mathcal{A}(p+1,h+1)}{gE-\mathcal{A}(p,h)}\right]^{n-1},\\ \omega_0(p,h,E) &= \frac{1}{2}g\frac{[gE-\mathcal{A}(p,h)]}{n}\\ &\quad\times[p(p-1)+4ph+h(h-1)],\\ \omega_-(p,h,E) &= \frac{1}{2}gph(n-2),\end{aligned} \tag{9}$$

where $\mathcal{A}(p,h)=(p^2+h^2+p-h)/4-h/2$. By neglecting the difference of matrix elements with different Δn, $M_+ = M_- = M_0 = M$, we estimate the value of M for a given nuclear state by associating the $\lambda_+(p,h,E)$ transitions with the probability for quasifree scattering of a nucleon above the Fermi level on a nucleon of the target nucleus. Therefore, we have

$$\begin{aligned}\frac{\langle\sigma(v_{\rm rel})v_{\rm rel}\rangle}{V_{\rm int}} &= \frac{\pi}{\hbar}|M|^2\frac{g[gE-\mathcal{A}(p+1,h+1)]}{n+1}\\ &\quad\times\left[\frac{gE-\mathcal{A}(p+1,h+1)}{gE-\mathcal{A}(p,h)}\right]^{n-1},\end{aligned} \tag{10}$$

where $V_{\rm int}$ is the interaction volume estimated as $V_{\rm int} = \frac{4}{3}\pi(2r_c+\lambda/2\pi)^3$, with the de Broglie wavelength $\lambda/2\pi$ corresponding to the relative velocity $v_{\rm rel}=\sqrt{2T_{\rm rel}/m_N}$. m_N is the mass of interacting excitons (nucleons) and $T_{\rm rel}$ is their relative kinetic energy. A value of the order of the nucleon radius is used for r_c in the CEM: $r_c = 0.6$ fm.

The averaging on the left-hand side of Eq. (10) is carried out over all excited states, taking into account the exclusion principle. Combining (8)–(10) we finally get for the transition rates

$$\begin{aligned}\lambda_+(p,h,E) &= \frac{\langle\sigma(v_{\rm rel})v_{\rm rel}\rangle}{V_{\rm int}},\\ \lambda_0(p,h,E) &= \frac{\langle\sigma(v_{\rm rel})v_{\rm rel}\rangle}{V_{\rm int}}\left[\frac{gE-\mathcal{A}(p,h)}{gE-\mathcal{A}(p+1,h+1)}\right]^{n+1}\\ &\quad\times\frac{n+1}{n}\frac{p(p-1)+4ph+h(h-1)}{gE-\mathcal{A}(p,h)},\\ \lambda_-(p,h,E) &= \frac{\langle\sigma(v_{\rm rel})v_{\rm rel}\rangle}{V_{\rm int}}\left[\frac{gE-\mathcal{A}(p,h)}{gE-\mathcal{A}(p+1,h+1)}\right]^{n+1}\\ &\quad\times\frac{ph(n+1)(n-2)}{[gE-\mathcal{A}(p,h)]^2}.\end{aligned} \tag{11}$$

The CEM predicts angular distributions for preequilibrium particles that are forward-peaked in the laboratory system. For instance, CEM03.03 assumes that a nuclear state with a given excitation energy E should be specified not only by the exciton number n but also by the momentum direction Ω. Following Ref. [50], the master equation [Eq. (3)] can be generalized for this case provided that the angular dependence for the transition rates λ_+, λ_0, and λ_- [Eq. (11)] may be factorized. In accordance with Eq. (10), in the CEM it is assumed that

$$\langle\sigma\rangle \to \langle\sigma\rangle F(\Omega), \tag{12}$$

where

$$F(\Omega) = \frac{d\sigma^{\rm free}/d\Omega}{\int d\Omega' d\sigma^{\rm free}/d\Omega'}. \tag{13}$$

The scattering cross section $d\sigma^{\rm free}/d\Omega$ is assumed to be isotropic in the reference frame of the interacting excitons, thus resulting in an asymmetry in both the nucleus center-of-mass and laboratory frames. The angular distributions of preequilibrium complex particles are assumed to be similar to those for the nucleons in each nuclear state [3].

This calculational scheme is easily realized by the Monte Carlo technique. It provides a good description of double-differential spectra of preequilibrium nucleons and a not-so-good but still reasonable description of complex-particle spectra from different types of nuclear reactions at incident energies from tens of MeV to several GeV.

For incident energies below about 200 MeV, Kalbach has developed a phenomenological systematics for preequilibrium-particle angular distributions by fitting available measured spectra of nucleons and complex particles [51]. As the Kalbach systematics are based on measured spectra, they describe very well the double-differential spectra of preequilibrium particles and generally provide a better agreement of calculated preequilibrium complex-particle spectra with data than does the CEM approach based on Eqs. (12) and (13). Therefore, CEM03.03 incorporates the Kalbach systematics [51] to describe angular distributions of both preequilibrium nucleons and complex particles at incident energies up to 210 MeV. At higher energies, CEM03.03 uses the CEM approach based on Eqs. (12) and (13).

As the MEM uses a Monte Carlo technique to solve the master equations describing the behavior of the nucleus at the preequilibrium stage (see details in Ref. [3]), it is relatively easy to extend the number of types of possible LF that can be emitted during this stage. For this, we have only to extend the loop in the CEM03.03 code calculating Γ_j for j from 1 to 6 (i.e., for the emission of n, p, d, t, ^{3}He, and ^{4}He) to a larger value, in this case, up to $j = 66$, to account for the possibility of preequilibrium emission of up to 66 types of particles and LF. Of course, in this extended loop, we have to calculate the emission width Γ_j for all j values. This entails calculating Coulomb barriers, binding energies, reduced masses, inverse cross sections, and condensation probabilities for all 66 types of particles and LF. As this extended CEM03.03 is intended to allow production of energetic light fragments, we subsequently refer to it as CEM03.03F, where "F" stands for energetic fragments. We also refer later to a similarly extended version of LAQGSM03.03 as LAQGSM03.03F. The list of all particles and LF that can be emitted during the preequilibrium stage of a nuclear reaction calculated with CEM03.03F is provided in Table I.

As can be seen from Eq. (5), the inverse cross sections used by these models at the preequilibrium stage (and at the evaporation/fission stage) have a significant impact on the calculated particle width, and affect greatly the final

TABLE I. The list of particles and light fragments that can be emitted during the preequilibrium stage of reactions in the extended MEM.

Z_j	Ejectiles						
0	n						
1	p	d	t				
2	^{3}He	^{4}He	^{6}He	^{8}He			
3	^{6}Li	^{7}Li	^{8}Li	^{9}Li			
4	^{7}Be	^{9}Be	^{10}Be	^{11}Be	^{12}Be		
5	^{8}B	^{10}B	^{11}B	^{12}B	^{13}B		
6	^{10}C	^{11}C	^{12}C	^{13}C	^{14}C	^{15}C	^{16}C
7	^{12}N	^{13}N	^{14}N	^{15}N	^{16}N	^{17}N	
8	^{14}O	^{15}O	^{16}O	^{17}O	^{18}O	^{19}O	^{20}O
9	^{17}F	^{18}F	^{19}F	^{20}F	^{21}F		
10	^{18}Ne	^{19}Ne	^{20}Ne	^{21}Ne	^{22}Ne	^{23}Ne	^{24}Ne
11	^{21}Na	^{22}Na	^{23}Na	^{24}Na	^{25}Na		
12	^{22}Mg	^{23}Mg	^{24}Mg	^{25}Mg	^{26}Mg	^{27}Mg	^{28}Mg

results and the accuracy of the MCNP6, MCNPX [52], and MARS15 [53] transport codes, which use these models as their event generators. This is why it is necessary to use as good as possible approximations for the inverse cross sections in the extended models.

The unmodified codes use the inverse cross sections $\sigma_{\rm inv}$, from Dostrovsky's formulas [54] for all emitted nucleons and the complex particles (d, t, ^{3}He, and ^{4}He):

$$\sigma_{\rm inv}(\epsilon) = \sigma_g \alpha \left(1 + \frac{\beta}{\epsilon}\right), \tag{14}$$

which is often written as

$$\sigma_{\rm inv}(\epsilon) = \begin{cases} \sigma_g c_n (1 + b/\epsilon) & \text{for neutrons,} \\ \sigma_g c_j (1 - V_j/\epsilon) & \text{for charged particles,} \end{cases}$$

where $\sigma_g = \pi R_d^2$ (fm^2) is the geometrical cross section. d denotes the "daughter" nucleus with mass and charge numbers A_d and Z_d produced from the "parent" nucleus i with mass and charge numbers A_i and Z_i after the emission of the particle j with mass and charge numbers A_j and Z_j and kinetic energy ϵ; $R_d = r_0 A_d^{1/3}$, and $r_0 = 1.5$ fm. α and β are defined as

$$\alpha = 0.76 + 2.2 A_d \text{ MeV},$$

$$\beta = \frac{2.12 A_d^{-2/3} - 0.05}{0.76 + 2.2 A_d^{-1/3}} \text{ MeV},$$

and c_j is estimated by interpolation of the tabulated values published in Ref. [54].

The Coulomb barrier (in MeV) is estimated as

$$V_j = k_j Z_j Z_d e^2 / R_c, \tag{15}$$

where $R_c = r_0 (A_d^{1/3} + A_j^{1/3})$, $r_0 = 1.5$ fm, and the penetrability coefficients k_j are calculated via interpolation of the tabulated values published in Ref. [54].

At the evaporation/fission stage of reactions described by CEM0.03 and LAQGSM0.03, which use an extension of the generalized evaporation model code GEM2 by Furihata [24], the inverse cross sections are calculated with the same functional form, but using different constants from those in the original approximations [54]. We label those different inverse cross sections as "GEM2."

The Dostrovsky model is very old. It was not intended for use above about 50 MeV/nucleon, and is not very suitable for emission of fragments heavier than ^{4}He. Better total-reaction cross-section models that can be used as an estimate for inverse cross sections are available today, most notably the NASA model [55], the approximations by Barashenkov and Polanski [56], and those by Kalbach [57]. A quite complete list of references on modern total-reaction cross-section models, as well as on recent publications where these models are compared with each other and with available experimental data, can be found in Ref. [34].

We have performed an extensive comparison of the NASA [55], Tsang *et al.* [58], Dostrovsky *et al.* [54], Barashenkov and Polanski [56], GEM2 [24], and Kalbach [57] systematics for total reaction (*inverse*) cross sections (see also the older works [13,59,60] with similar comparisons). We conclude that the NASA approach is superior, in general, to the other available models (see Ref. [13,34,59,60] for the details of these findings). This is why we implement the NASA inverse cross sections into the MEM to be used at the preequilibrium stage of reactions.

The NASA approximation as described by Eq. (16) attempts to simulate several quantum-mechanical effects, such as the optical potential for neutrons (with the parameter X_m) and collective effects such as Pauli blocking through the quantity δ_T (for more details, see Refs. [55]);

$$\sigma_{\rm NASA} = \pi r_0^2 \left(A_P^{1/3} + A_T^{1/3} + \delta_T\right)^2 \left(1 - R_c \frac{B_T}{T_{cm}}\right) X_m, \tag{16}$$

where r_0, A_P, A_T, δ_T, R_c, B_T, T_{cm}, and X_m are a constant used to calculate the radii of nuclei, the mass number of the projectile nucleus, the mass number of the target nucleus, an energy-dependent parameter, a system-dependent Coulomb multiplier, the energy-dependent Coulomb barrier, the colliding system center-of-momentum energy, and an optical model multiplier used for neutron-induced reactions, respectively.

In the case of neutron-induced reactions, we cannot use the unmodified NASA systematics to approximate the inverse cross sections for neutrons, as that model, while being much better at predicting the total reaction cross section throughout most of the energy region of the data, falls to zero at low energies. Since neutrons have no Coulomb barrier and are emitted at even very low energies, a finite neutron cross section at very low energies is needed. For these low-energy neutrons, we use the Kalbach systematics [57], which prove to be a very good approximation for the inverse cross sections of low-energy neutrons, as discussed in Refs. [13,34,61]. In CEM03.03F, we use the Kalbach systematics [57] to replace the NASA inverse cross sections [55] for low-energy neutrons, similar to what was suggested and done in Ref. [13] for the code CEM2k. In other words, at neutron energies around the maximum cross section and below, the calculation uses Kalbach systematics, and switches to the NASA model for the higher neutron-energy range. The Kalbach systematics are scaled in CEM03.03F to match the NASA model results at

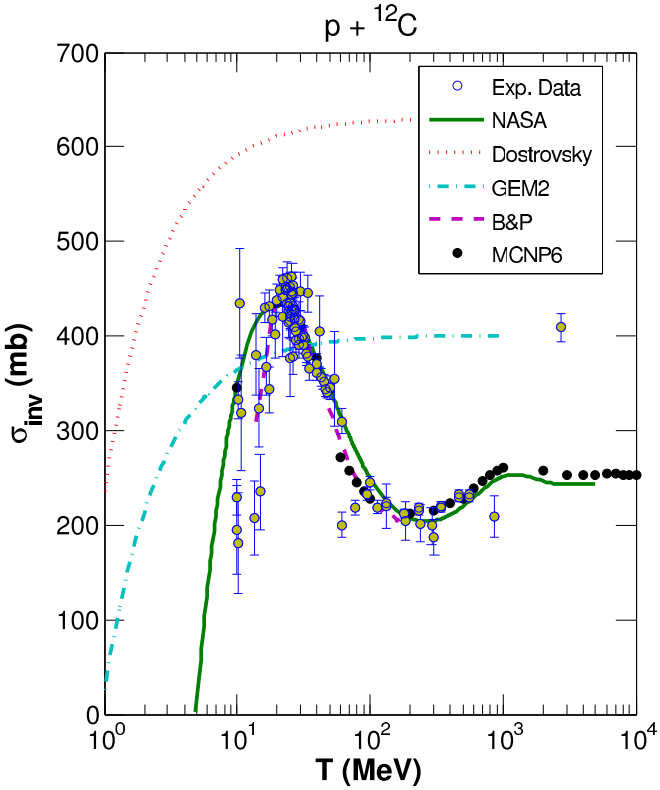

FIG. 5. Reaction cross section for $p + {}^{12}\mathrm{C}$, as calculated by the NASA, Dostrovsky, GEM2, and BP models (solid and broken lines). The black dots are cross sections calculated by MCNP6, and the circles are experimental data [62].

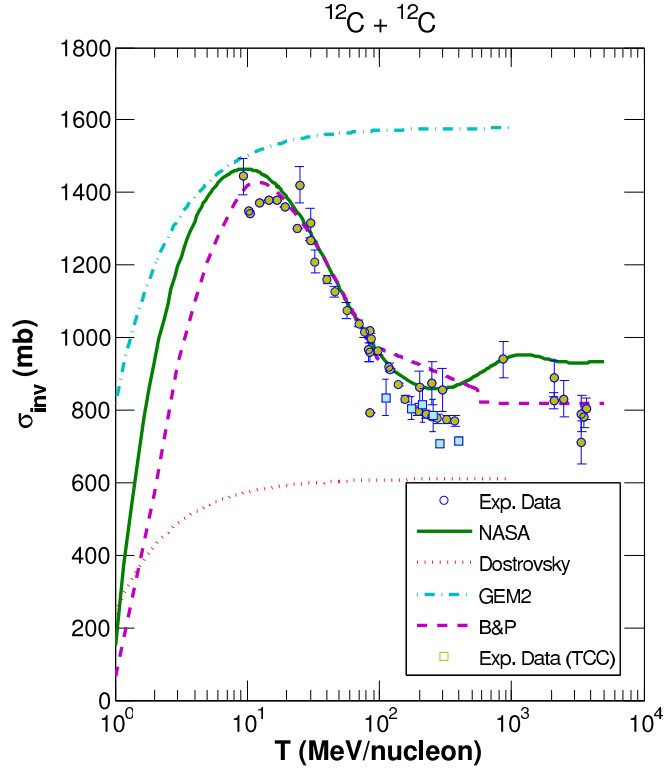

FIG. 6. Reaction cross section for ${}^{12}\mathrm{C} + {}^{12}\mathrm{C}$ as calculated by the NASA, Dostrovsky, GEM2, and BP models (solid and broken lines). The circles are experimental data [63] and the squares are total charge-changing cross section (TCC) measurements [64].

the transition point (depending on the nucleus) so as not to have a discontinuity. Transition points and scaling factors are obtained for all possible residual nuclei, by mass number; they are fixed in the code and are used in all subsequent calculations. (Reference [61] provides tables of these.)

Examples of inverse cross sections for the emission of neutrons together with discussions and relevant references can be found in Refs. [13,34,61]. We limit ourselves to one example with inverse cross sections for the emission of protons, and one example of inverse cross section for ${}^{12}\mathrm{C}$.

Figure 5 illustrates calculated total reaction cross sections for $p + {}^{12}\mathrm{C}$ using the NASA, Dostrovsky, GEM2, and Barashenkov and Polanski (BP) models, compared to calculations by MCNP6 and experimental data. The NASA model appears to be superior to the Dostrovsky-like models.

Figure 6 displays the total reaction cross section for ${}^{12}\mathrm{C} + {}^{12}\mathrm{C}$, as calculated by the NASA, Dostrovsky, GEM2, and BP models, compared to experimental data and to measured total charge-changing (TCC) cross sections. TCC cross sections should be 5–10% less than total reaction cross sections, as TCC cross sections do not include neutron removal. The NASA cross-section model fits the experimentally measured data, in general, better than the other models tested. See Ref. [61] for results of other heavy-ion-induced reactions.

Many similar results for the emission of nucleons, complex particles, and LF heavier than ${}^{4}\mathrm{He}$ can be found in Refs. [13,34,59,61].

The partial transmission probability λ_j, the probability that an ejectile of the type j will be emitted with kinetic energy T, is given in Eq. (5). This form is valid only for neutrons and protons. An extended form appropriate for the case of complex particles and LF is (see Ref. [3])

$$\lambda_j(p,h,E,T) = \gamma_j \frac{2s_j+1}{\pi^2\hbar^3}\mu_j \Re(p,h)\frac{\omega(p_j,0,T+B_j)}{g_j} \times \frac{\omega(p-p_j,h,E-B_j-T)}{\omega(p,h,E)} T\sigma_j^{\mathrm{inv}}(T), \tag{17}$$

where

$$g_j = \frac{V(2\mu_j)^{3/2}}{4\pi^2\hbar^3}(2s_j+1)(T+B_j)^{1/2}. \tag{18}$$

Details on Eq. (18) can be found in Ref. [65]. γ_j is the probability that the proper number of particle excitons will coalesce to form a type j fragment (also called γ_β in a number of earlier publications; see, e.g., Refs. [65–67]).

In the standard CEM03.03, the Dostrovsky form of the inverse cross section is simple enough so that for neutrons and protons the integral from Eq. (4) can be done analytically. However, for complex particles, the level density ω becomes too complicated (see details in Refs. [2–4]); therefore, the

integral is evaluated numerically. In this case, a six-point Gauss-Legendre quadrature is used when the exciton number is 15 or less, and a 6-point Gauss-Laguerre quadrature is used when the number of excitons is greater than 15.

We adopt for CEM03.03F the NASA form of the cross sections, which removes the possibility of analytic integration, so the integral is always calculated numerically. We use an eight-point Gauss-Legendre quadrature when the number of excitons is 15 or less, and an eight-point Gauss-Laguerre quadrature when the number of excitons is greater than 15. (See Ref. [34] for details.)

These integration methods are sufficient for these models because individual Γ_j precision is not extremely important for choosing what type of particle/LF j will be emitted. In contrast to analytical preequilibrium models, the Monte Carlo method employed by CEM uses the ratios of Γ_j to the sum of Γ_j over all j. That is, if we estimate all Γ_j with the same percentage error, the final choice of the type j of particle/LF to be emitted as simulated by CEM would be the same as if we would calculate all Γ_j exactly. We think that this is the main reason why CEM provides quite reasonable results using the old Dostrovsky approximation for inverse cross sections, in spite of the significant difference of the Dostrovsky inverse cross sections from those now used. The ratios of the individual widths to the total width were approximated better than each individual width, because the errors in each channel have the same sign. This is illustrated in Fig. 5. (See more examples and discussion in Ref. [34].)

We observe that the condensation probability γ_j could be calculated more physically from first principles, if one were studying only this problem. But such a calculation is not feasible in these event generators given practical Monte Carlo computational time limitations. γ_j is, therefore, estimated as the overlap integral of the wave function of independent nucleons with that of the complex particle (see details in Ref. [3]), as shown in Eq. (6).

As noted above, Eq. (6) is a rather crude estimate. As is frequently done (see e.g., Refs. [65,67]), the values of γ_j are taken from fitting the theoretical preequilibrium spectra to the experimental ones. In CEM03.03F, to improve the description of preequilibrium complex-particle emission, we estimate γ_j by multiplying the estimate provided by Eq. (6) by empirical coefficients $F_j(A,Z,T_0)$, whose values are fitted to available nucleon-induced experimental complex-particle spectra. Therefore, the new equation for γ_j using this empirical coefficient is

$$\gamma_j = F_j p_j^3 \left(\frac{p_j}{A}\right)^{p_j-1}. \tag{19}$$

The values of F_j for d, t, ^{3}He, and ^{4}He used by the original CEM03.03 need to be refitted after the current upgrades to the inverse cross sections and the coalescence model (discussed below). Then, values of F_j need to be obtained for heavy clusters up to ^{28}Mg, once the model is extended to emit these heavy clusters. This was done for all possible target nuclei. We have developed a universal approximation, or a "numerical model," for $F_j(A,Z,T_0)$ to be used in CEM03.03F. All details of this part of our work can be found in Refs. [39,40,61].

Once a fragment of type j has been randomly chosen for emission, the kinetic energy of this fragment needs to be determined. This is done by sampling the kinetic energy from the λ_j distribution, Eq. (17), using the NASA cross section as the $\sigma_j^{\rm inv}(T)$.

The energy dependence of λ_j for the new inverse cross sections is more complicated than that that arising from the simple Dostrovsky form used in the original CEM03.03. This affects the method we choose to randomly sample T_j ($\equiv T$) from the correct spectrum.

To sample T_j uniformly from the λ_j distribution using the Monte Carlo method, we must first find the maximum of λ_j. In CEM03.03, this is done analytically using the derivative of λ_j with respect to T_j, due to the simple nature of the energy dependence in the Dostrovsky systematics. The NASA cross section energy dependence is much more complicated; therefore, we find the maximum of λ_j numerically using the golden-section method. This also provides us the flexibility to modify the cross-section model in the future without needing to modify the kinetic energy algorithm.

After finding the maximum value of λ_j, the kinetic energy of the emitted fragment j is uniformly sampled from the λ_j distribution using the rejection technique from a gamma distribution (shape parameter $\alpha = 2$) as the comparison function. (See Ref. [68] for a description of the gamma distribution.)

Figure 57 of Ref. [61] illustrates results for the probability of emitting ^{6}Li with a given kinetic energy $T_{\rm Li}$ simulated by CEM03.03F and the original CEM03.03. Probabilities from the λ_j distributions with the NASA inverse cross sections differ slightly from those with the Dostrovsky inverse cross sections, just as expected. Technical details with many illustrative figures on this part of our work can by found in Refs. [39,61].

V. COALESCENCE MODEL

As previously described, one of the three possible mechanisms CEM and LAQGSM use to produce energetic LF is the coalescence of nucleons emitted during the INC as well as of already coalesced lighter fragments into heavier clusters.

When the cascade stage of a reaction is completed, CEM03.03 and LAQGSM03.03 use the coalescence model described in Refs. [69,70] to "create" high-energy d, t, ^{3}He, and ^{4}He by final-state interactions among emitted cascade nucleons, already outside of the target nucleus. In contrast to most other coalescence models for heavy-ion-induced reactions, where complex-particle spectra are estimated simply by convolving the measured or calculated inclusive spectra of nucleons with corresponding fitted coefficients, CEM03.03 and LAQGSM03.03 use in their simulations of particle coalescence real information about all emitted cascade nucleons and do not use integrated spectra. These models assume that all the cascade nucleons having differences in their momenta smaller than p_c and the correct isotopic content form an appropriate composite particle. This means that the formation probability for, e.g., a deuteron is

$$W_d(\vec{p},b) = \iint d\vec{p}_p d\vec{p}_n \rho^C(\vec{p}_p,b)\rho^C(\vec{p}_n,b) \times \delta(\vec{p}_p + \vec{p}_n - \vec{p})\Theta(p_c - |\vec{p}_p - \vec{p}_n|), \tag{20}$$

where the particle density in momentum space is related to the one-particle distribution function f by

$$\rho^C(\vec{p},b) = \int d\vec{r}\, f^C(\vec{r},\vec{p},b). \quad (21)$$

Here, b is the impact parameter for the projectile interacting with the target nucleus and the superscript index C shows that only cascade nucleons are taken into account for the coalescence process. The coalescence radii p_c were fitted for each composite particle in Ref. [69] to describe available data for the reaction Ne+U at 1.04 GeV/nucleon, but the fitted values turned out to be quite universal and were subsequently found to satisfactorily describe high-energy complex-particle production for a variety of reactions induced both by particles and nuclei at incident energies up to about 400 GeV/nucleon, when describing nuclear reactions with different versions of LAQGSM [5,6,59] or with its predecessor, the quark-gluon string model (QGSM) [29]. These parameters (in units of MeV/c) are

$$p_c(d) = 90, \quad p_c(t) = p_c(^3\mathrm{He}) = 108, \quad p_c(^4\mathrm{He}) = 115. \quad (22)$$

As the INC of CEM is different from those of LAQGSM or QGSM, it is natural to expect different best values for p_c as well. Recent studies have shown (see, e.g., Refs. [2,4] and references therein) that the values of parameters p_c defined by Eq. (22) are also good for CEM03.03 for projectile particles with kinetic energies T_0 lower than 300 MeV and equal to or above 1 GeV. For incident energies in the interval 300 MeV $< T_0 \leqslant 1$ GeV, a better overall agreement with the available experimental data is obtained by using values of p_c equal to 150, 175, and 175 MeV/c for d, t (^{3}He), and ^{4}He, respectively. These values of p_c are fixed as defaults in CEM03.03. If several cascade nucleons are chosen to coalesce into composite particles, they are removed from the distributions of nucleons and do not contribute further to such nucleon characteristics as spectra, multiplicities, etc.

In comparison with the initial version [69,70], in CEM03.03 and LAQGSM03.03, several coalescence routines have been changed and have been tested against a large variety of measured data on nucleon- and nucleus-induced reactions at different incident energies. Many examples with results by CEM03.03 and LAQGSM03.03 for reactions where the contribution from the coalescence mechanism is important and can be easily seen may be found in, e.g., Refs. [4,22].

Note that following the coalescence idea used by these models, the latest versions of the INCL code (e.g., [10]) also consider (by different means) the coalescence of nucleons in the very outskirts of the nuclear surface into light fragments during the INC stages of reactions. In a way, the coalescence of INCL is similar to the one considered by CEM and LAQGSM as proposed in Ref. [69,70], with the main difference being that INCL considers coalescence of INC nucleons on the border of a nucleus, just barely inside the target nucleus, while CEM and LAQGSM coalesce INC nucleons and lighter clusters already outside the nucleus.

The standard "03.03" versions of both CEM and LAQGSM consider coalescence of only d, t, ^{3}He, and ^{4}He. Here we extend the coalescence model in CEM to account for the coalescence of heavier clusters, with mass numbers up to $A = 7$ in CEM, and up to $A = 12$ in LAQGSM. The extended coalescence model of CEM is described below, while the one of LAQGSM, in the next section.

The coalescence model of CEM first checks all nucleons to form two-nucleon pairs, as their their momenta permit. It then checks if an α particle can be formed from two two-nucleon pairs (either from two n-p pairs or from an n-n and a p-p pair). After this it checks to see if any of the two-nucleon pairs left can combine with another nucleon to form either tritium or ^{3}He. Last, it checks to see if any of these three-nucleon groups (tritium or ^{3}He) can coalesce with another nucleon to form ^{4}He.

The extended coalescence model takes these two-nucleon pairs, three-nucleon (tritium or ^{3}He only) groups, and ^{4}He to see if they can coalesce to form heavier clusters. ^{4}He can coalesce with a three-nucleon group to form either ^{7}Be or ^{7}Li. Two three-nucleon groups can coalesce to form either ^{6}Li or ^{6}He, and ^{4}He can coalesce with a two-nucleon pair to form either ^{6}Li or ^{6}He. All coalesced nucleons are removed from the distributions of nucleons and lighter fragments so that the coalescence model conserves both atomic and mass numbers. For additional details of the extended coalescence model in CEM, see Ref. [71].

p_c determines how dissimilar the momenta of nucleons can be and still coalesce. Naturally, after the extension of the coalescence model in CEM to account for LF heavier than ^{4}He, we had to redefine p_c, to include a value for heavy clusters, or LF: p_c(LF). In CEM03.03F, the new p_c's for incident energies, T, less than 300 MeV or greater than 1000 MeV are

$$p_c(d) = 90\,\mathrm{MeV}/c, \quad p_c(t) = p_c(^3\mathrm{He}) = 108\,\mathrm{MeV}/c,$$
$$p_c(^4\mathrm{He}) = 130\,\mathrm{MeV}/c, \quad p_c(\mathrm{LF}) = 175\,\mathrm{MeV}/c. \quad (23)$$

For 300 $< T <$ 1000 MeV they are

$$p_c(d) = 150\,\mathrm{MeV}/c, \quad p_c(t) = p_c(^3\mathrm{He}) = 175\,\mathrm{MeV}/c,$$
$$p_c(^4\mathrm{He}) = 205\,\mathrm{MeV}/c, \quad p_c(\mathrm{LF}) = 250\,\mathrm{MeV}/c. \quad (24)$$

$p_c(^4\mathrm{He})$ was increased compared to the original p_c values defined by Eq. (22) because too many α particles were lost (coalesced into heavy clusters); therefore, this was compensated for by coalescing more ^{4}He.

As an example, Fig. 7 displays experimental measurements of the reaction 480 MeV $p + {}^{\mathrm{nat}}\mathrm{Ag} \rightarrow {}^6\mathrm{Li}$ by Green *et al.* [72], compared with simulations from CEM03.03F without the coalescence extension (i.e., with the extended preequilibrium model and improved inverse cross sections but using the old coalescence model), CEM03.03F with the coalescence extension, and the original CEM03.03. Even without the coalescence extension, CEM03.03F (which contains the extended preequilibrium model and improved inverse cross sections) yields much better results than the original CEM03.03 without these improvements. Adding the coalescence extension produces even better results.

This example also highlights how coalescence can produce heavy clusters not only at high energies, but also at low and moderate energies, thus improving agreement with experimental data in all these energy regions.

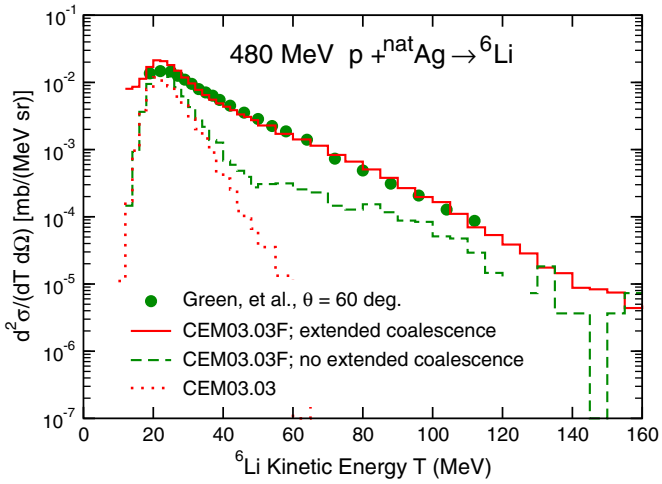

FIG. 7. Comparison of experimental measurements of the reaction 480 MeV $p + {}^{\text{nat}}\text{Ag} \rightarrow {}^{6}\text{Li}$ at 60° by Green *et al.* [72] (green circles), with simulations from the original CEM03.03 (red dotted line), CEM03.03F without the coalescence extension (green dashed line), and CEM03.03F with the coalescence extension (red solid line).

Similar results for many other reactions where the coalescence mechanism is important and easily seen can be found in Refs. [39,40,71].

VI. LAQGSM EXTENSION

LAQGSM [4–6] is a very powerful predictive tool for heavy-ion-induced reactions and/or nuclear reactions induced by particles at high energies (> several GeV/nucleon). MCNP6 uses it as its default event generator to simulate all heavy-ion-induced reactions as well as reactions induced by particles at energies above 4.5 GeV (above 1.2 GeV, in the case of photonuclear reactions).

The INC of LAQGSM03.03 is described with a recently improved version [6,73] of the time-dependent intranuclear cascade model developed initially at JINR in Dubna, often referred to in the literature as the Dubna intranuclear cascade model, DCM (see [69] and references therein). The DCM models interactions of fast cascade particles ("participants") with nucleon spectators of both the target and projectile nuclei and includes as well interactions of two participants (cascade particles). It uses experimental particle+particle cross sections at energies below 4.5 GeV/nucleon, or those calculated by the quark-gluon string model (QGSM) at higher energies (see, e.g., Ref. [74] and references therein) to simulate angular and energy distributions of cascade particles, and also considers the Pauli exclusion principle.

After the INC, LAQGSM03.03 uses the same preequilibrium, coalescence, Fermi breakup, and evaporation/fission models as described above for CEM (with some parameters different from the ones used by CEM, because the INC of LAQGSM is completely different from the INC of CEM; see more details in Ref. [4]).

As examples, Figs. 8–10 show results for three reactions simulated by LAQGSM compared with available experimental data, to illustrate the predictive power of LAQGSM03.03 used

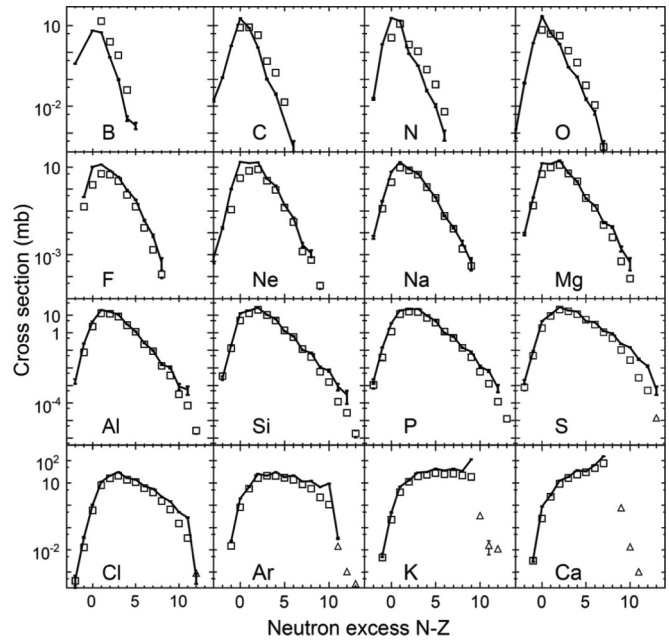

FIG. 8. Measured elemental cross sections for ^{48}Ca fragmentation on ^{9}Be at 140 MeV/nucleon [75] (open symbols) compared to LAQGSM03.03 predictions (solid lines).

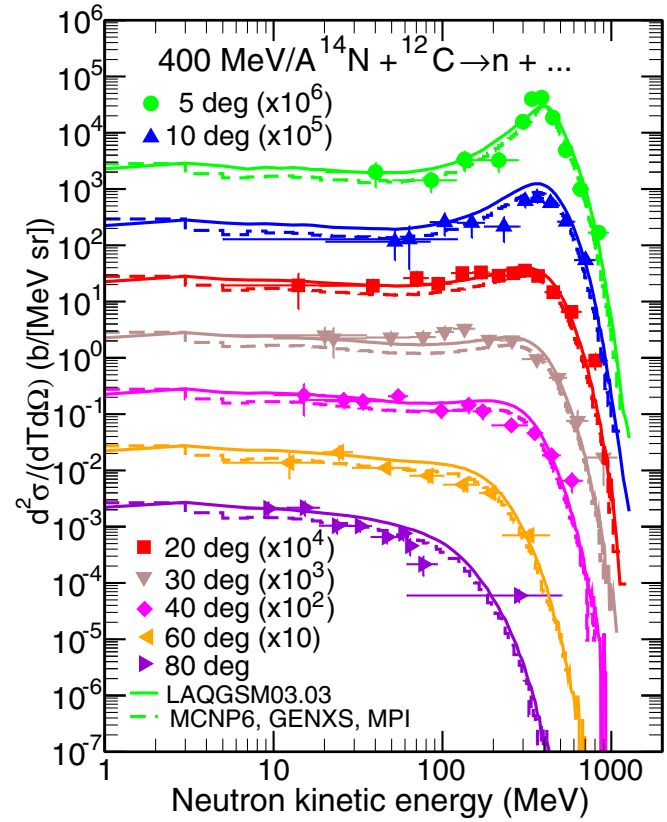

FIG. 9. Experimental neutron spectra from 400 MeV/nucleon ^{14}N+^{12}C [76] (solid symbols), compared with calculations by the production version of MCNP6 (dashed lines) and by the LAQGSM03.03 event generator used as a stand-alone code (solid lines).

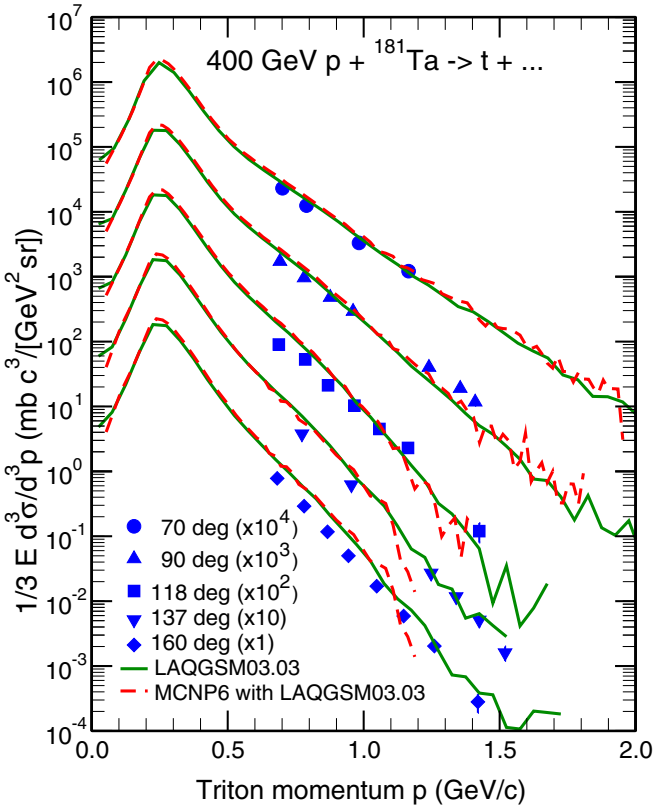

FIG. 10. Experimental invariant spectra of tritons from the reaction 400 GeV $p + {}^{181}$Ta [77] (solid symbols), compared with results by LAQGSM03.03 [6] used as a stand-alone code (solid lines) and by MCNP6 using the LAQGSM03.03 event generator (dashed lines).

as the default event generator in MCNP6 for these types of reactions. The data in Figs. 8 and 9 were made available after LAQGSM03.03 was developed.

Figure 8 shows an example of elemental product yields measured by Mocko *et al.* [75] from the fragmentation of ^{48}Ca on ^{9}Be at 140 MeV/nucleon. Many similar results for other reactions can be found in Ref. [6].

Figure 9 displays experimental neutron spectra from 400 MeV/nucleon ^{14}N + ^{12}C [76], compared with calculations by MCNP6 and the LAQGSM03.03 event generator used as a stand-alone code. Such data are of significant interest for applications related to cancer treatment with carbon beams, and most of the neutron spectra from such reactions were measured at the Heavy-Ion Medical Accelerator in the Chiba facility (HIMAC) of the Japanese National Institute of Radiological Science (NIRS). We obtained similar agreement by LAQGSM and by MCNP6 using LAQGSM for many similar reactions, at different incident energies and for different projectile-target nuclear combinations (see Ref. [23]).

Figure 10 shows that LAQGSM predicts well light cluster spectra even at the ultrarelativistic energies of 400 GeV. Similar results for other ejectiles from such reactions can be found in Ref. [22].

In CEM03.03F, we extend the coalescence model to account for heavier fragments up to ^{7}Be. As CEM is restricted to simulate only particle-induced reactions, and only at energies below about 5 GeV, such an extension of the coalescence model may be sufficient. Since LAQGSM is used to calculate also reactions induced by heavy ions, and at much higher incident energies, where the mean multiplicities of the secondary

TABLE II. Coalescence channels (modes) for LF produced in the extended coalescence model of LAQGSM03.03F; values of p_c are listed in units of MeV/c per nucleon).

LF	p_c	Channels (modes)				
d	90	$p+n$				
t	108	$d+n$				
^{3}He	108	$d+p$				
^{4}He	115	^{3}He $+n$	$t+p$	$d+d$		
^{6}He	150	$t+t$				
^{6}Li	150	$t+{}^{3}$He	^{4}He $+d$			
^{7}Li	150	$t+{}^{4}$He	^{6}Li $+n$			
^{8}Li	150	^{7}Li $+n$	^{6}He $+d$			
^{9}Li	150	^{8}Li $+n$	^{6}He $+t$			
^{7}Be	150	^{3}He $+{}^{4}$He	^{6}Li $+p$			
^{9}Be	150	^{8}Li $+p$	^{7}Li $+d$			
^{10}Be	150	^{9}Be $+n$	^{8}Li $+d$			
^{10}B	150	^{9}Be $+p$	^{7}Li $+{}^{3}$He	^{6}Li $+{}^{4}$He		
^{11}B	150	^{10}B $+n$	^{9}Be $+d$	^{7}Li $+{}^{4}$He		
^{12}B	150	^{11}B $+n$	^{10}Be $+d$	^{8}Li $+{}^{4}$He		
^{11}C	150	^{10}B $+p$	^{7}Be $+{}^{4}$He			
^{12}C	150	^{11}C $+n$	^{11}B $+p$	^{10}B $+d$	^{9}Be $+{}^{3}$He	^{6}Li $+{}^{6}$Li

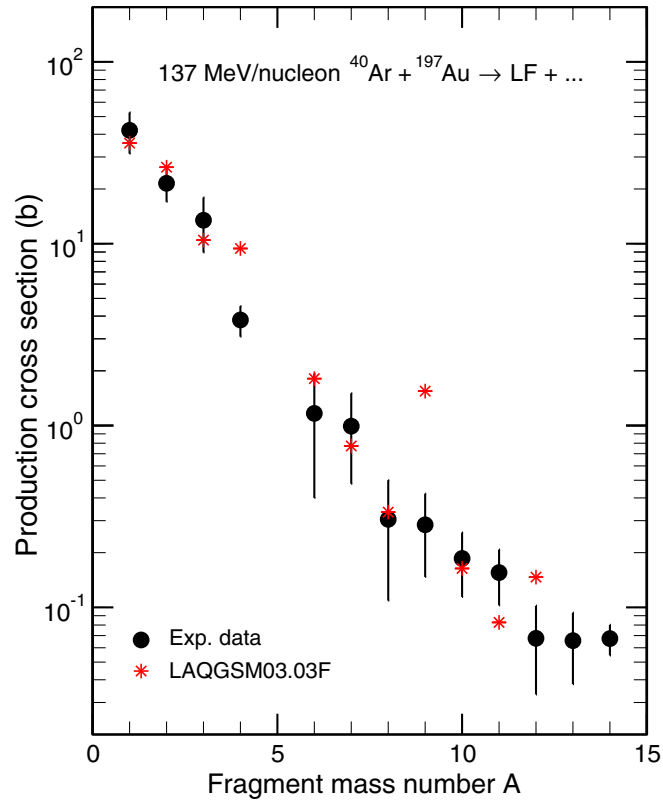

FIG. 11. Measured cross sections for light fragments produced in 137 MeV/nucleon ^{40}A + ^{197}Au reactions [78] (black circles), compared to predictions by LAQGSM03.03 with the extended coalescence model (red stars).

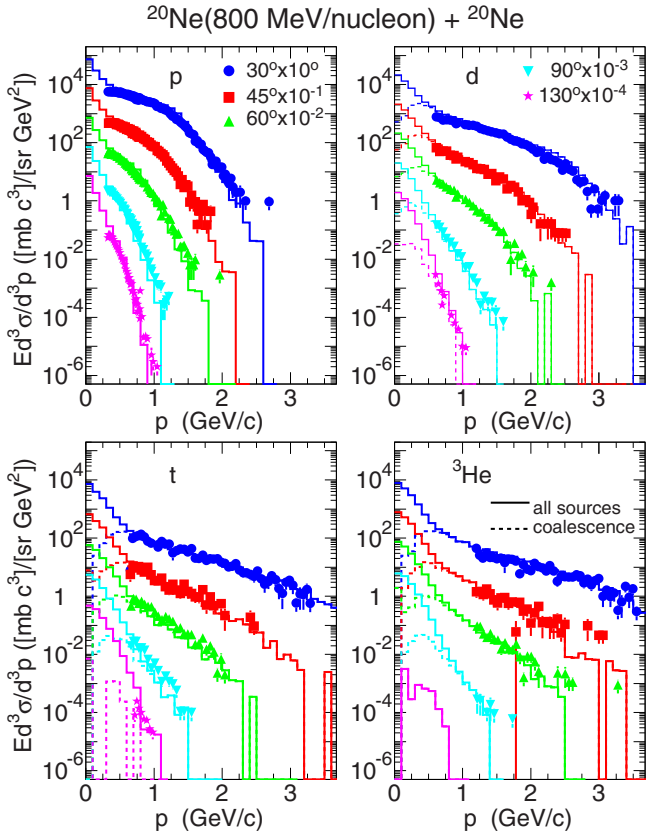

FIG. 12. Experimental invariant p, d, t, and ^{3}He spectra at 30, 45, 60, 90, and 130 degrees (symbols) from a thin NaF target bombarded with an 800 MeV/nucleon ^{20}Ne beam [80] (solid points), compared with results by LAQGSM03.03 using the extended coalescence model (histograms). The calculations were performed for ^{20}Ne + ^{20}Ne.

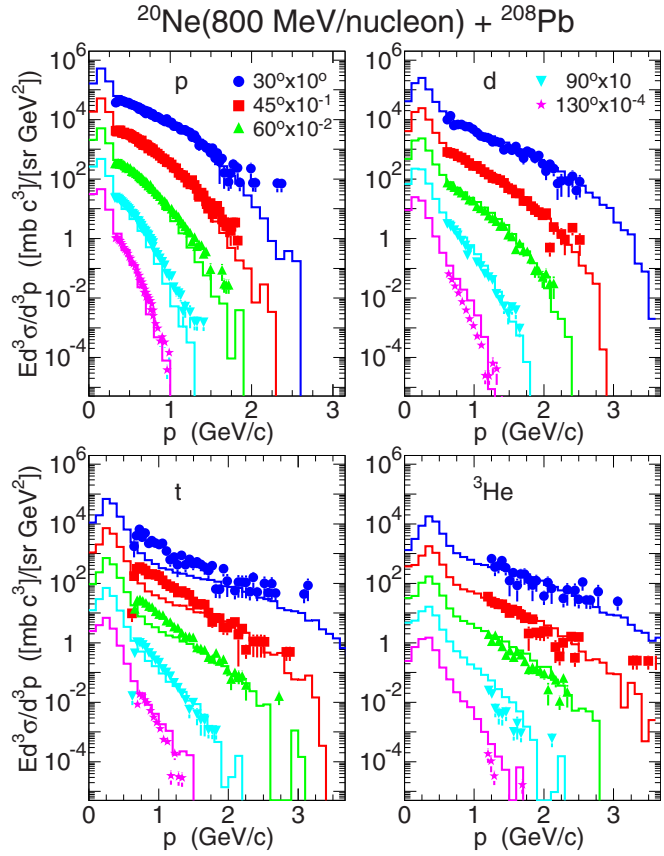

FIG. 13. Experimental invariant p, d, t, and ^{3}He spectra at 30, 45, 60, 90, and 130 degrees from a thin Pb target bombarded with an 800 MeV/nucleon ^{20}Ne beam [80] (symbols), compared with results from LAQGSM03.03 using the extended coalescence model (histograms).

nucleons and LF are much higher than for reactions simulated with CEM, we extend the coalescence model in LAQGSM to even heavier LF, up to ^{12}C. Table II shows the LF we produce via the extended coalescence model in LAQGSM, and the real channels (modes) we consider to form each LF. The values of p_c used in the extended LAQGSM are also listed; they differ slightly from the ones used by CEM03.03F.

Figure 11 provides an example of preliminary results for the case of fragment-production cross sections as functions of mass number, measured by Jacak *et al.* at the LBL BEVALAC for 137 MeV/nucleon beams of ^{40}Ar bombarding ^{197}Au targets [78], compared to LAQGSM03.03F results obtained with the extended coalescence model (but still using the old preequilibrium model). There is reasonably good agreement with experimental data for mass numbers up to $A = 12$, except for $A = 9$.

Figures 12 and 13 show two more examples of results obtained with the extended coalescence model in LAQGSM, namely, invariant cross section for the production of p, d, t, and ^{3}He at 30, 45, 60, 90, and 130 deg from 800 MeV/nucleon ^{20}Ne + ^{20}Ne and ^{208}Pb, respectively. There is a very good agreement of results by the extended LAQGSM03.03F with these experimental data. We obtain similar results for several other similar reactions measured at Berkeley and published in Ref. [80].

The LAQGSM03.03F extension is still a work in progress. We have extended and frozen its coalescence model, but so far have implemented only the extended preequilibrium model, exactly as it was developed for CEM03.03F, with the same parameters. Figures 14 and 15 show two examples by this preliminary version of LAQGSM03.03F, namely, spectra of ^{6,7,8,9}Li at 65° from proton-gold interactions at 1.2 and 1.9 GeV, respectively. This preliminary version of LAQGSM03.03F describes quite well spectra of all Li fragments measured for these reactions by the PISA Collaboration and published in Ref. [20]. LAQGSM03.03F produces similar results for other LF, from other target nuclei, and at other incident energies measured by the PISA Collaboration. However, as Figs. 14 and 15 indicate, a fine-tuning of several parameters in the extended preequilibrium model (and perhaps the values of p_c in the extended coalescence model) would improve the agreement of the results with these measured data. We hope to perform such a fine-tuning in the future and to validate LAQGSM03.03F on as many measured reactions as possible, before implementing it into MCNP6 to replace the current version of LAQGSM03.03.

To demonstrate the reliability of even this nonoptimized version of LAQGSM03.03F for predicting unmeasured reactions, we compare the code predictions to some recently

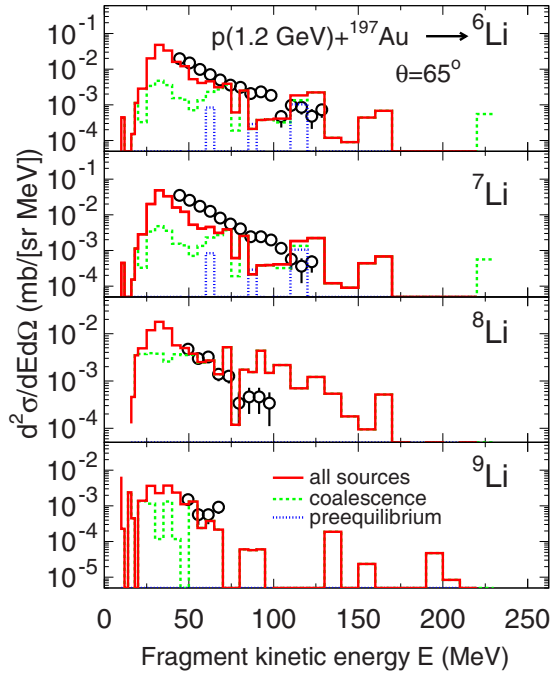

FIG. 14. Comparison of the experimental data for ^{6,7,8,9}Li spectra at 65° produced from 1.2 GeV protons incident on ^{197}Au [20] (open circles), compared to results calculated by the preliminary LAQGSM03.03F (histograms). The dotted and dashed histograms show the contributions from the preequilibrium emission and the extended coalescence model, respectively.

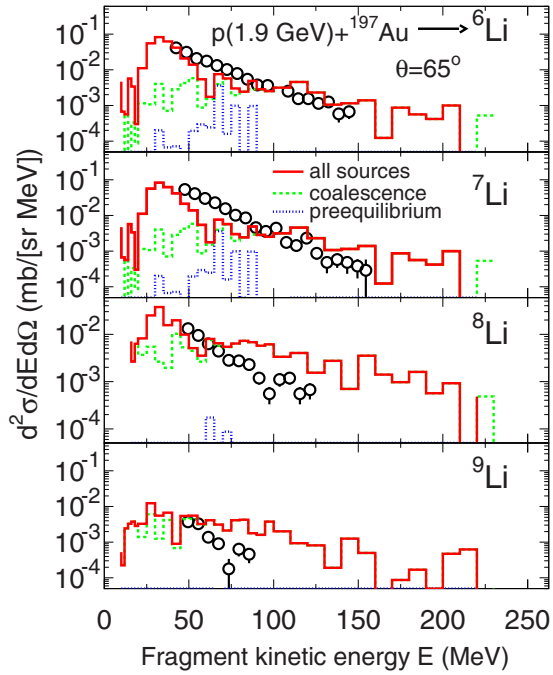

FIG. 15. Comparison of the experimental data for ^{6,7,8,9}Li spectra at 65° produced from 1.9 GeV protons incident on ^{197}Au [20] (open circles), compared to results calculated by the preliminary LAQGSM03.03F (histograms). The dotted and dashed histograms show the contributions from the preequilibrium emission and the extended coalescence model, respectively.

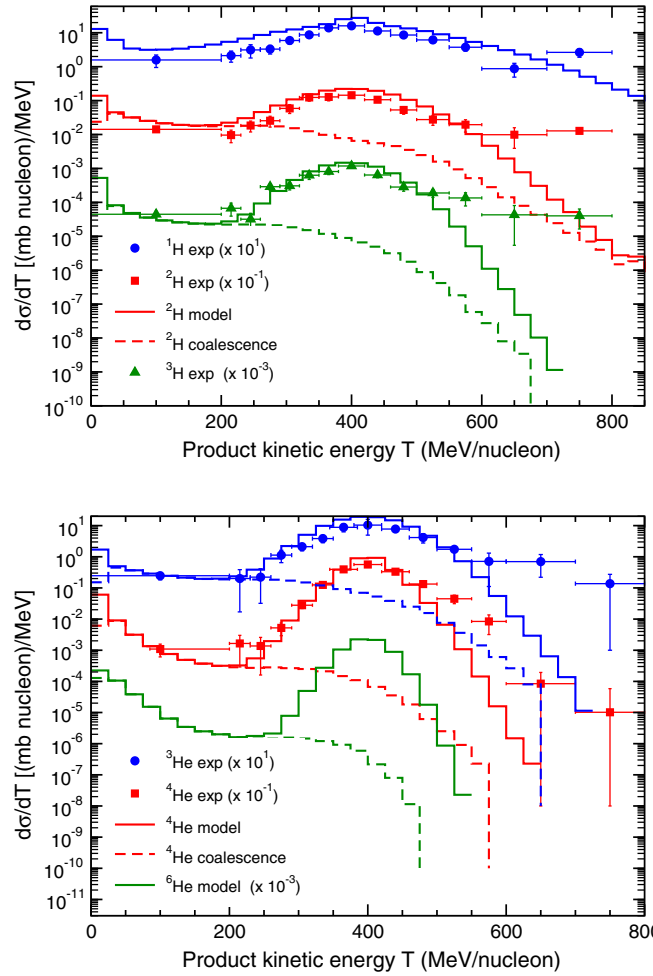

FIG. 16. Comparison of recently measured product spectra at forward laboratory angles ($\theta \leqslant 6°$) from the fragmentation of 400 MeV/nucleon ^{12}C projectiles on a ^{197}Au target into H and He isotopes [79] (symbols), compared with results from the previously fixed preliminary LAQGSM03.03F code (solid lines). The model results from the coalescence mechanism alone are shown by dashed lines.

measured data that were made available only after the code was put into its current form. We show in Figs. 16 and 17 the measured forward-scattered fragmentation products from the interaction of ^{12}C nuclei at 400 MeV per nucleon with a ^{197}Au target [79]. The measured cross sections are very well predicted, except for the very highest energies, where the nucleons in these fragments have momenta more than 100 MeV/c above the momentum of the original nucleons from the ^{12}C projectiles. This discrepancy may indicate effects of high-momentum components which are known to exist in real nuclei, and which are missing from the simple semiclassical nucleon momentum distributions assumed in the existing Fermi breakup model.

VII. VALIDATION OF THE EXTENDED MODELS

After extending the preequilibrium and coalescence models in CEM03.03F, we have analyzed a number of nuclear

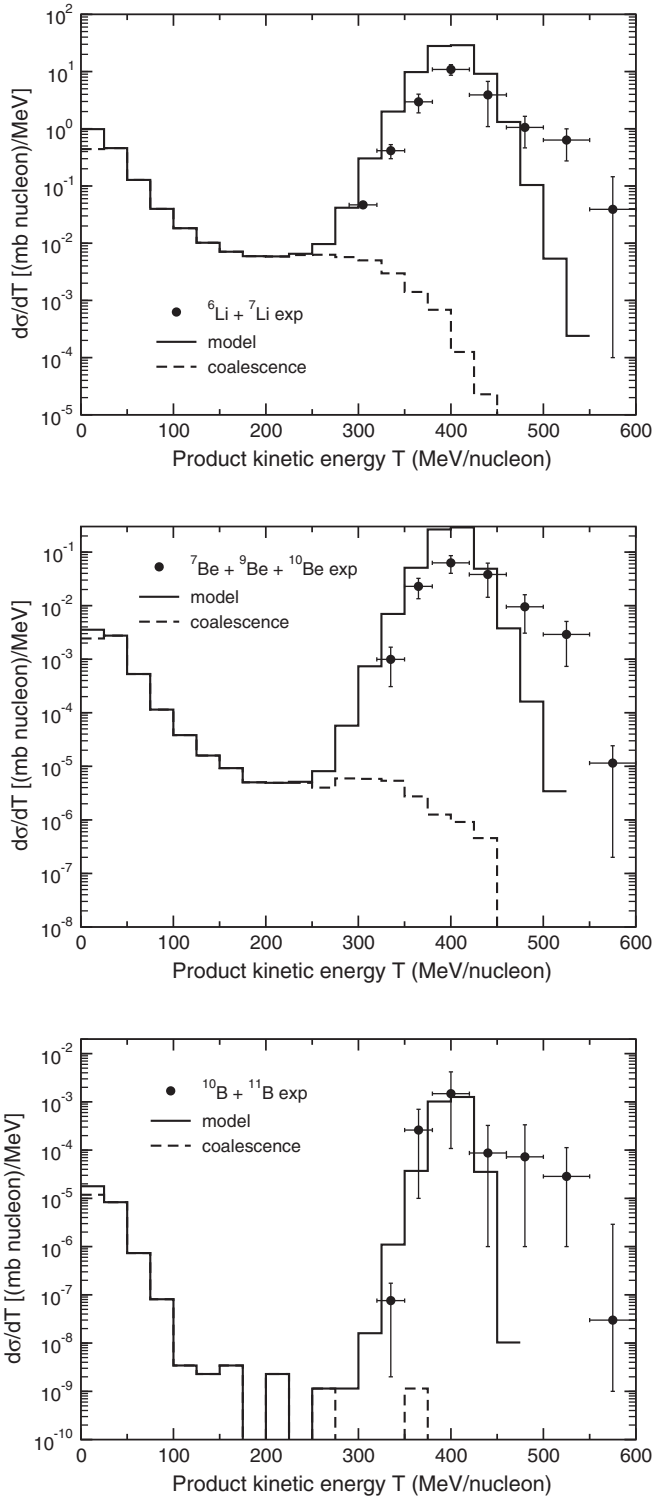

FIG. 17. Same as Fig. 16 for production of Li, Be, and B isotopes.

reactions using different values for A_{Fermi} in the Fermi breakup model discussed in Sec. III, and have concluded that generally a better agreement with most of the experimental data so far analyzed is obtained with $A_{\mathrm{Fermi}} = 12$, the same value as used in the original 03.03 versions of CEM and LAQGSM. This value is used for the extended "F" versions of these models.

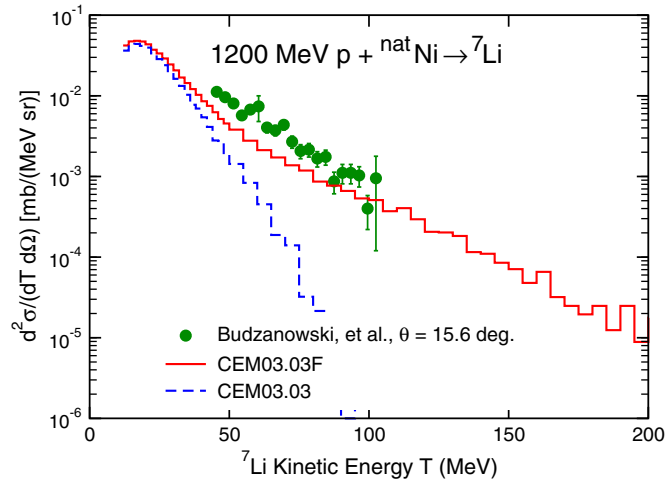

FIG. 18. Comparison of experimental data for 1200 MeV $p + {}^{\mathrm{nat}}\mathrm{Ni} \rightarrow {}^{7}\mathrm{Li}$ at 15.6°, measured by Budzanowski *et al.* [21] (solid circles), to results from the original CEM03.03 (dashed line) and to those from the improved CEM03.03F (solid line).

An example of calculations with the final version of CEM03.03F is shown in Fig. 18, which compares experimental data for the ^{7}Li spectrum at 15.6° from 1.2 GeV $p + \mathrm{Ni}$ [21] with results from CEM03.03 and CEM03.03F. Similar results from MCNP6 are presented below in Sec. VIII. More extensive results can be found in Ref. [39]. CEM03.03F has much improved results compared to the original CEM03.03, especially for heavy-cluster spectra.

Before implementing the extended "F" versions of the models into the MCNP6 transport code, we have tested that the new models do not "destroy" the good predictive power and agreement with available experimental data provided by the original CEM03.03 and LAQGSM03.03 event generators, considering reactions previously well modeled and not used directly in the current developments of the preequilibrium and coalescence models. This is to verify that the extended "F" models have similar good predictive powers as previously established for the original event generators. We show only a few examples from this extensive effort.

Figure 19 demonstrates this for 317 MeV $n + {}^{209}\mathrm{Bi} \rightarrow t$ at 54°, with experimental data measured by Franz *et al.* [81]. We have obtained similar results for other neutron-induced reactions, at other incident energies, for other ejectiles and target nuclei. These results illustrate that the improved production of heavy clusters in CEM03.03F has not destroyed the spectra of particles and LF of mass 4 and below from neutron-induced reactions, not considered during this development of the "F" code versions.

Figures 20 and 21 compare examples of experimental data for γ- and π-induced reactions to results from CEM03.03 and CEM03.03F.

Figure 20 shows the results for 300 MeV $\gamma + {}^{\mathrm{nat}}\mathrm{Cu} \rightarrow p$ at 45°, 90°, and 135° compared to experimental data by Schumacher *et al.* [82].

Figure 21 shows the model results for 1500 MeV $\pi^{+} + {}^{\mathrm{nat}}\mathrm{Fe} \rightarrow n$ at 30°, 90°, and 150°, compared to experimental data from Nakamoto *et al.* [83]. The last two figures

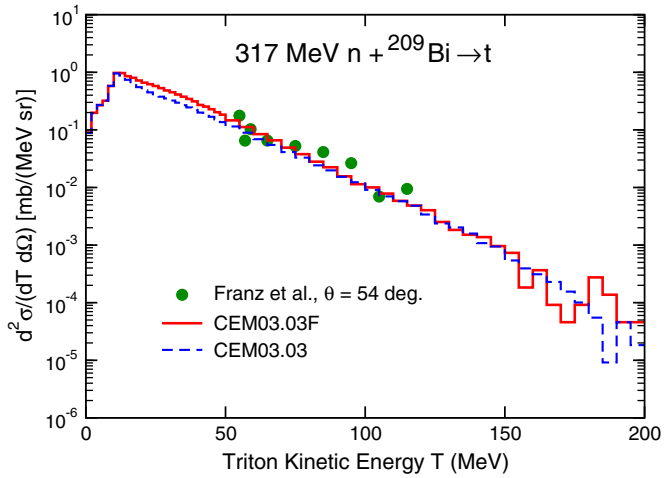

FIG. 19. Comparison of experimental data for 317 MeV $n + {}^{209}\mathrm{Bi} \rightarrow t$ at 54° measured by Franz *et al.* [81] (solid circles) to results from the original CEM03.03 (solid lines) and from the improved CEM03.03F (dashed lines).

provide examples of the consistency between CEM03.03F and CEM03.03 for ejectile spectra from γ- and π-induced reactions.

Figure 22 shows the measured [84] mass and charge distributions of the product yields from the reaction 800 MeV $p + {}^{197}\mathrm{Au}$, the mean kinetic energy of these products, and the mass distributions of the cross sections for the production of thirteen elements with atomic number Z from 20 to 80, compared to predicted results from the original CEM03.03 and from CEM03.03F. The results are essentially identical for the two code versions for these observables.

Figure 23 shows the measured [85,86] fission cross sections for $n + \mathrm{Bi}$ as a function of neutron energy, compared to results from CEM03.03 and CEM03.03F. CEM03.03F agrees reasonably well with these new data on $n + \mathrm{Bi}$ fission cross sections, even showing an improvement around energies of 100 MeV, while seeming to slightly underpredict the experiments above about 300 MeV. But because CEM03.03F considers emission of LF at the preequilibrium stage, there is some relative depletion from the compound nucleus cross section, and the mean values of A, Z, and E of the fissioning nuclei differ slightly from the corresponding values in CEM03.03. All details of the extended GEM2 code used in CEM and LAQGSM to calculate σ_f can be found in Refs. [2,4,24]. In the case of subactinide nuclei, the main parameter that determines fission cross sections calculated by GEM2 is the level-density parameter in the fission channel, a_f (or more exactly, the ratio a_f/a_n, where a_n is the level-density parameter for neutron evaporation). Ideally, the empirical a_f/a_n parameter in CEM03.03F should be refit to reflect the changed average properties of the fissioning compound nuclei following the preequilibrium decay. This effort lies outside the scope of this report, which is focused on energetic LF emission.

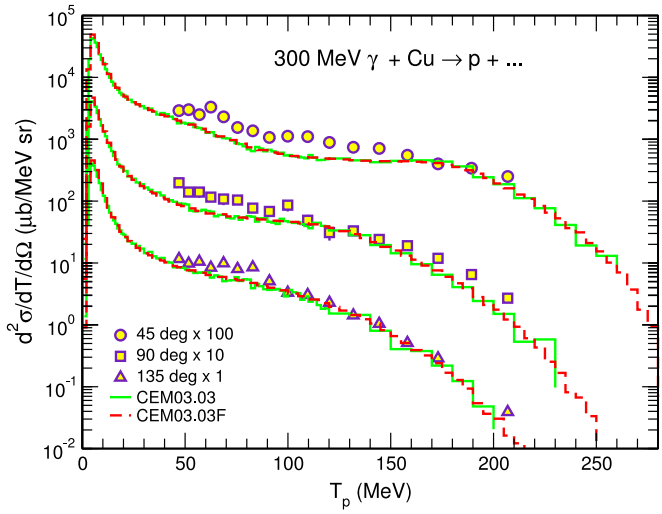

FIG. 20. Experimental data for 300 MeV $\gamma + {}^{\mathrm{nat}}\mathrm{Cu} \rightarrow p$ at 45°, 90°, and 135° from Schumacher *et al.* [82] (open symbols), compared to results from the unmodified CEM03.03 (solid lines) and to those from CEM03.03F (dashed lines).

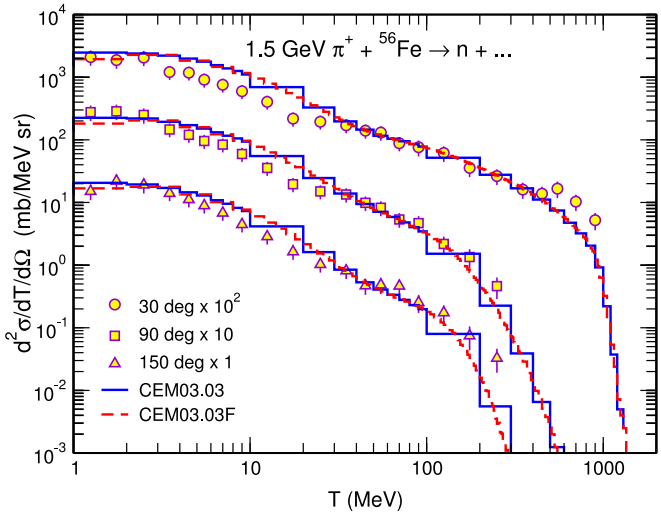

FIG. 21. Comparison of experimental data for 1500 MeV $\pi^+ + {}^{\mathrm{nat}}\mathrm{Fe} \rightarrow n$ at 30°, 90°, and 150° from Nakamoto *et al.* [83] (open symbols) to results from the unmodified CEM03.03 (solid lines) and to CEM03.03F (dashed lines).

As CEM03.03 is the default event generator within MCNP6 for energies above 150 MeV, its ability to run simulations quickly is important. We tested the impact of the current improvements on the computation time with each incremental upgrade, and found either no significant increase or only a small increase in the computation time. We tested also the cumulative effect of all of the improvements on the computation time. Adding all of the upgrades increases the computation time by approximately one-third, depending upon the incident energy and target nucleus. Considering the comprehensive nature of the upgrades, and the dramatic improvements made to the description of heavy cluster production, this seems to be a relatively tolerable increase.

VIII. IMPLEMENTATION INTO MCNP6

As mentioned in the Introduction, MCNP6 is a general-purpose Monte Carlo radiation-transport code used by several

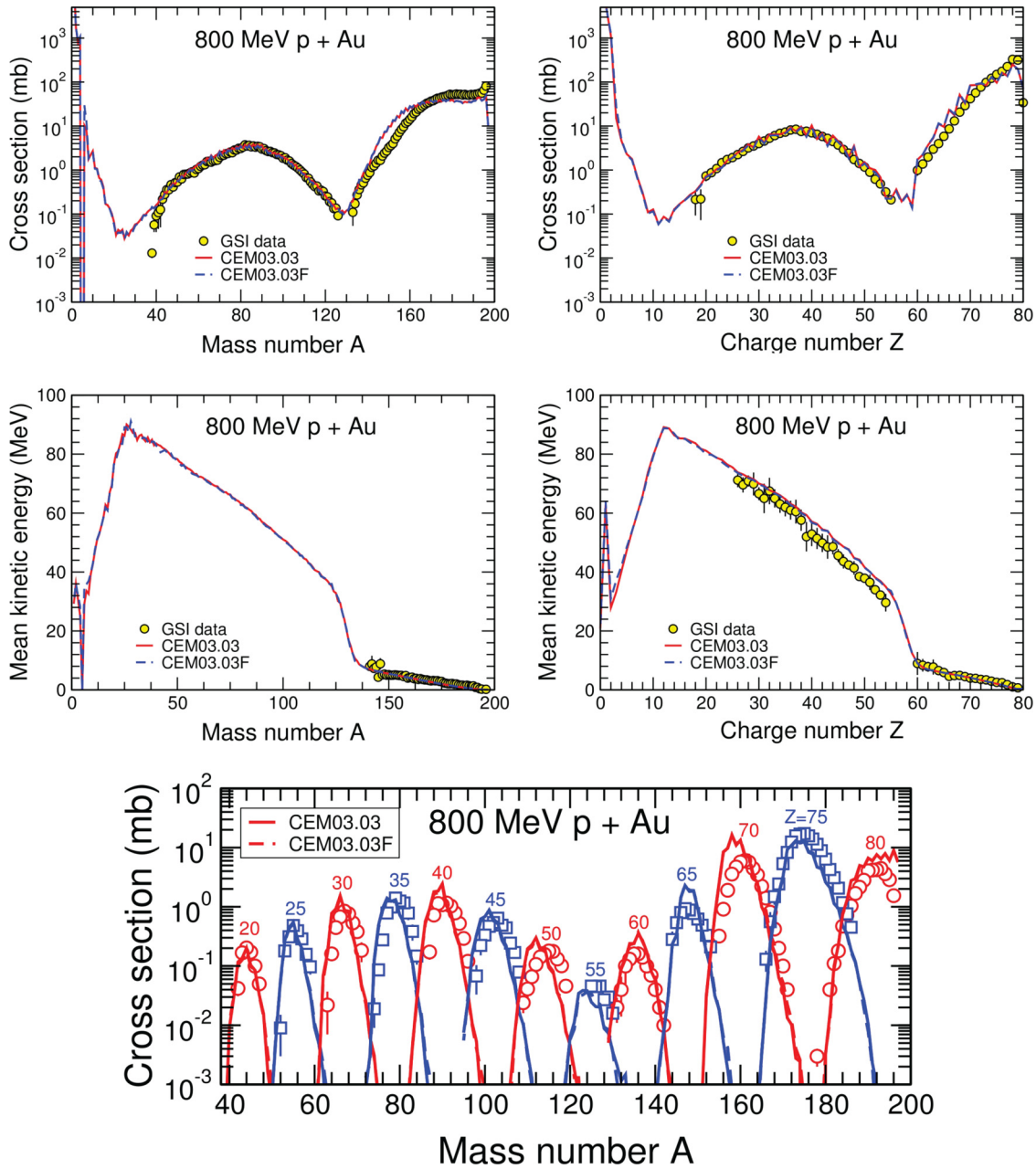

FIG. 22. Comparison of measured mass and charge distributions of the product yields from the reaction 800 MeV $p + {}^{197}$Au, the mean kinetic energies of these products, and the mass distributions of the cross sections for the production of thirteen elements with atomic numbers Z ranging from 20 to 80 [84] (open symbols), to predicted results from the original CEM03.03 (solid lines) and from CEM03.03F (dashed lines).

thousands of individuals or groups to simulate various nuclear applications. But MCNP6 can be and is actually used also in academic studies, e.g., to simulate experimental facilities or only some of their parts, such as target stations, or to estimate some unmeasured cross sections. The easiest way to calculate with MCNP6 the absolute values of spectra of ejectiles and/or yields of reaction products is by using its so-called GENXS option (e.g., [1,87]).

Previously, double differential cross sections of ejectiles could be calculated by MCNP6 using the GENXS option only for elementary particles and very light fragments up to ^{4}He. Thus, a necessary first step in implementing the improved CEM03.03F into MCNP6 involves extending the ability to output spectra of heavy clusters.

We have extended the GENXS option [88]. This GENXS upgrade includes the ability to calculate (or, to "tally," in the language used by MCNP6) and output double differential cross sections for any fragment or heavy ion. This upgrade also includes the ability to tally and output angle-integrated cross sections as a function of emitted fragment energy and

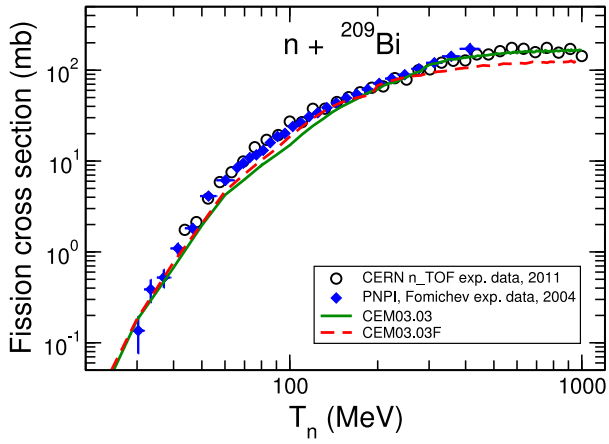

FIG. 23. Comparison of measured fission cross sections for n + Bi [85] (open circles) and [86] (solid diamonds) to results from the unmodified CEM03.03 (solid line) and from CEM03.03F (dashed lines).

energy-integrated cross sections as a function of emitted angle, for any products. More details on using this GENXS extension can be found in Refs. [39,88].

After completing and testing the improved CEM03.03F, and after extending the GENXS option of MCNP6, we inserted CEM03.03F to replace the older CEM03.03 event generator into a working test version of MCNP6, called MCNP6-F. Two of the current improvements are always implemented in MCNP6-F: the upgraded NASA-Kalbach inverse cross sections in the preequilibrium stage, and the new energy-dependent γ_j numerical model. The other two improvements (extension of preequilibrium emission to ^{28}Mg, and the extension of the coalescence model to ^{7}Be), both of which increase slightly the computation time, may be turned off if desired. We also introduced a new input variable to specify the number of types of preequilibrium and coalescence fragments to be considered. The default of MCNP6-F is to consider the full upgrade of CEM03.03F as described above, i.e., up to 66 types of preequilibrium particle and LF and up to $A = 7$ in the coalescence model. But if a user wishes to save about 1/3 of the computing time, this input parameter may be given a value of 6, to consider emission of only n, p, d, t, ^{3}He, and ^{4}He, as done in the original CEM03.03. As mentioned in the previous section, LAQGSM03.03F is still under development, and is not yet implemented into MCNP6-F; this will be done in the future, after the completion and validation of LAQGSM03.03F.

We have tested MCNP6-F on a large number of various reactions. A very few examples from this validation work are presented below.

Figure 24 illustrates the results for 1200 MeV $p + {}^{197}$Au $\rightarrow {}^{6}$Li at 20°, with experimental data by Budzanowski *et al.* [20]. This figure provides additional evidence that MCNP6-F demonstrates increased production of heavy clusters in the

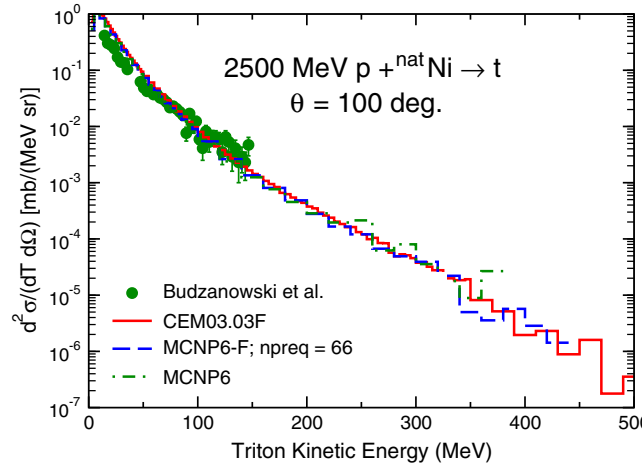

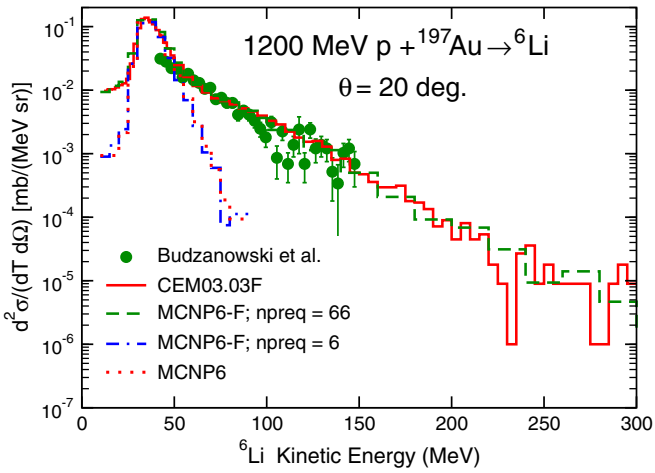

FIG. 24. Comparison of experimental data on 1200 MeV $p + {}^{197}$Au $\rightarrow {}^{6}$Li at 20°, measured by Budzanowski *et al.* [20] (solid circles), to calculated results by CEM03.03F (red solid line), MCNP6-F with npreqtyp = 66 (dashed green line), MCNP6-F with npreqtyp = 6 (dash-dash-dotted blue line), and the original MCNP6 with the GENXS extension only (red dotted line).

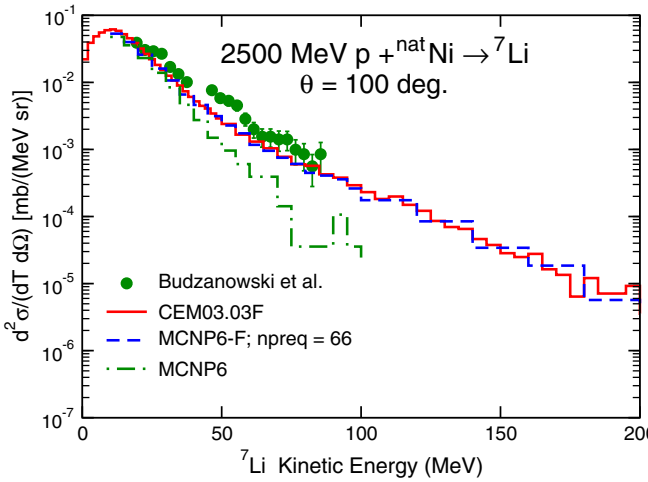

FIG. 25. Comparison of experimental data for 2500 MeV $p + {}^{\text{nat}}$Ni $\rightarrow t, {}^{7}$Li at 100°, measured by Budzanowski *et al.* [21] (solid circles), to calculated results from CEM03.03F (solid red lines), MCNP6-F with npreqtyp= 66 (dashed blue lines), and the original MCNP6 with the GENXS extension only (dash-dotted green lines).

mid- and high-energy regions compared to the original MCNP6. This reaction also highlights the need to improve the evaporation model used by CEM: The peak of the spectrum is too high; such peaks are largely produced by evaporation. We expect that this situation might be improved by implementing the improved inverse cross sections already incorporated into the preequilibrium model into the evaporation model, and hope to do such work in the future. We note there is a recent work on improving the Liège INC to its INCL4.6 version by Boudard *et al.* [10], which obtained similar results for heavy-cluster spectra from this reaction using INCL4.6 + ABLA07.

Figure 25 demonstrates the results for 2500 MeV $p + {}^{\rm nat}{\rm Ni} \rightarrow t, {}^{7}{\rm Li}$ at 100°, compared to experimental data measured by Budzanowski *et al.* [21]. The triton spectra again illustrate that MCNP6-F achieves increased production of heavy clusters without "destroying" the established spectra of nucleons and LF with $A < 5$.

Many more similar results on the validation of the extended MCNP6-F for other reactions can be found in Refs. [39,40].

IX. CONCLUSIONS

We have presented the results of our work to improve the description of energetic light-fragment production by the CEM and LAQGSM models, and by the Los Alamos MCNP6 transport code from various nuclear reactions at energies up to ∼1 TeV/nucleon.

In these models, energetic LF can be produced via Fermi breakup, preequilibrium emission, and coalescence mechanisms. We extend the modified exciton model used by CEM03.03 to describe emission of preequilibrium particles to account for a possibility of multiple emission of up to 66 types of particles and LF (up to ^{28}Mg) at the preequilibrium stage of reactions. For this extension, we had to develop an approximation, or a "numerical model," to calculate the probability γ_j of several excited nucleons to condense into a fragment of the type j inside the nucleus, that can be emitted at the preequilibrium stage of a reaction.

We have also improved the calculation of inverse cross sections at the preequilibrium stage of reactions, with a new hybrid NASA-Kalbach approach, instead of using the old Dostrovsky model which was used previously. This extended version of the MEM is implemented into the upgraded CEM, labeled CEM03.03F, as well as into a new LAQGSM03.03F.

Then, we extended the coalescence models in these codes to account for coalescence of LF from nucleons emitted at the intranuclear cascade stage of reactions and from lighter clusters, up to fragments with mass numbers $A \leqslant 7$, in the case of CEM, and $A \leqslant 12$, in the case of LAQGSM. Finally, we studied several variations of the Fermi breakup model and chose the option with the best overall performance to use in the production versions of the models.

We have tested the improved versions of CEM and LAQGSM on a variety of nuclear reactions induced by nucleons, pions, photons, and heavy ions. On the whole, the improved models describe much better than the original "03.03" versions production of energetic fragments heavier than ^{4}He, without "destroying" the good agreement provided by the standard versions for the emission of nucleons, light complex particles, and residual nuclei.

Next, we extended MCNP6 to allow calculation of and outputting of spectra of fragments and heavier products with arbitrary mass and charge numbers.

Last, we implemented the improved CEM03.03F into MCNP6, producing an upgraded version called MCNP6-F. LAQGSM03.03F is not complete and will be incorporated into MCNP6-F at a later time. We have validated MCNP6-F on a variety of measured nuclear reactions.

We conclude that the improved CEM, LAQGSM, and MCNP6 allow us to describe energetic LF from particle- and nucleus-induced reactions and provide a good agreement with available experimental data. They have a good predictive power for various reactions at energies up to ∼1 TeV/nucleon and can be used as reliable tools in applications involving such types of nuclear reactions as well as in scientific studies.

For future work, we hope to complete the development of LAQGSM03.03F and to implement it into MCNP6. We also hope to develop a better deexcitation (evaporation/fission + multifragmentation) model for both the CEM and LAQGSM event generators by incorporating the new inverse cross section approximations developed for and employed in the preequilibrium model.

ACKNOWLEDGMENTS

We are grateful to Dr. Christopher Werner and Dr. Avneet Sood of the Los Alamos National Laboratory for encouraging discussions and support. This study was carried out under the auspices of the National Nuclear Security Administration of the US Department of Energy at Los Alamos National Laboratory under Contract No. DE-AC52-06NA25396. This work was supported in part (for L.M.K.) by the M. Hildred Blewett Fellowship of the American Physical Society, http://www.aps.org.

[1] T. Goorley, M. James, T. Booth, F. Brown, J. Bull, L. J. Cox, J. Durkee, J. Elson, M. Fensin, R. A. Forster, J. Hendricks, H. G. Hughes, R. Johns, B. Kiedrowski, R. Martz, S. Mashnik, G. McKinney, D. Pelowitz, R. Prael, J. Sweezy, L. Waters, T. Wilcox, and T. Zukaitis, Nucl. Technol. **180**, 298 (2012).

[2] S. G. Mashnik and A. J. Sierk, CEM03.03 User Manual, LANL Report LA-UR-12-01364, Los Alamos, 2012; https://mcnp.lanl.gov/

[3] K. K. Gudima, S. G. Mashnik, and V. D. Toneev, Nucl. Phys. A **401**, 329 (1983).

[4] S. G. Mashnik, K. K. Gudima, R. E. Prael, A. J. Sierk, M. I. Baznat, and N. V. Mokhov, CEM03.03 and LAQGSM03.03 Event Generators for the MCNP6, MCNPX, and MARS15 Transport Codes, LANL Report LA-UR-08-2931, Los Alamos, 2008, arXiv:0805.0751.

[5] K. K. Gudima, S. G. Mashnik, and A. J. Sierk, User Manual for the Code LAQGSM, LANL Report LA-UR-01-6804, Los Alamos, 2001, https://mcnp.lanl.gov/

[6] S. G. Mashnik, K. K. Gudima, N. V. Mokhov, and R. E. Prael, LAQGSM03.03 Upgrade and Its Validation, LANL Report LA-UR-07-6198, Los Alamos, 2007; arXiv:0709.1736.

[7] H. W. Bertini, Phys. Rev. **131**, 1801 (1963); **188**, 1711 (1969).

[8] Y. Yariv and Z. Fraenkel, Phys. Rev. C **20**, 2227 (1979).

[9] A. Boudard, J. Cugnon, S. Leray, and C. Volant, Phys. Rev. C **66**, 044615 (2002).

[10] A. Boudard, J. Cugnon, S. Leray, and C Volant, Nucl. Phys. A **740**, 195 (2004); D. Mancusi, A. Boudard, J. Cugnon, J.-C. David, P. Kaitaniemi, and S. Leray, Phys. Rev. C **90**, 054602 (2014).

[11] A. V. Konobeyev and Y. A. Korovin, Kerntechnik **60**, 14 (1995).

[12] Y. Uozumi, P. Evtoukhovitch, H. Fukuda, M. Imamura, H. Iwamoto, V. Kalinikov, W. Kallies, N. Khumutov, T. Kin, N. Koba, Y. Koba, N. Kuchinski, A. Moisenko, D. Mzavia, M. Nakano, V. Samoilov, Z. Tsamalaidze, G. Wakabayashia, and Y. Yamaxhita, Nucl. Instrum. Methods A **571**, 743 (2007).

[13] S. G. Mashnik, A. J. Sierk, and K. K. Gudima, Complex Particle and Light Fragment Emission in the Cascade-Exciton Model of Nuclear Reactions, LANL Report LA-UR-02-5185, Los Alamos, 2002; arXiv:nucl-th/0208048.

[14] E. Fermi, Prog. Theor. Phys. **5**, 570 (1950).

[15] J. Bondorf, A. Botvina, A. Iljinov, I. Mishustin, and K. Sneppen, Phys. Rep. **257**, 133 (1995).

[16] J. Aichelin, Phys. Rep. **202**, 233 (1991).

[17] D. Filges and F. Goldenbaum, *Handbook of Spallation Research: Theory, Experiments and Applications* (Wiley-VCH Verlag, Wennheim, 2009).

[18] J.-C. David, Eur. Phys. J. A **51**, 157 (2015).

[19] H. Machner, D. G. Aschman, K. Baruth-Ram, J. Carter, A. A. Cowley, F. Goldenbaum, B. M. Nangu, J. V. Pilcher, E. Sideras-Haddad, J. P. F. Sellschop, F. D. Smit, B. Spoelstra, and D. Steyn, Phys. Rev. C **73**, 044606 (2006).

[20] A. Budzanowski, M. Fidelus, D. Filges, F. Goldenbaum, H. Hodde, L. Jarczyk, B. Kamys, M. Kistryn, S. Kistryn, S. Kliczewski, A. Kowalczyk, E. Kozik, P. Kulessa, H. Machner, A. Magiera, B. Piskor-Ignatowicz, K. Pysz, Z. Rudy, R. Siudak, and M. Wojciechowski, Phys. Rev. C **78**, 024603 (2008).

[21] A. Budzanowski, M. Fidelus, D. Filges, F. Goldenbaum, H. Hodde, L. Jarczyk, B. Kamys, M. Kistryn, S. Kistryn, S. Kliczewski, A. Kowalczyk, E. Kozik, P. Kulessa, H. Machner, A. Magiera, B. Piskor-Ignatowicz, K. Pysz, Z. Rudy, R. Siudak, and M. Wojciechowski, Phys. Rev. C **82**, 034605 (2010).

[22] S. G. Mashnik, Eur. Phys. J. Plus **126**, 49 (2011).

[23] S. G. Mashnik, JPS Conf. Proc. **6**, 030143 (2015).

[24] S. Furihata, Nucl. Instr. Meth. B **171**, 252 (2000); Ph.D. thesis, Tohoku University, Sendai, Japan, 2003 (unpublished).

[25] V. S. Barashenkov and V. D. Toneev, *Interaction of High Energy Particle and Nuclei with Atomic Nuclei* (Atomizdat, Moscow, 1972).

[26] V. S. Barashenkov, A. S. Iljinov, N. M. Sobolevskii, and V. D. Toneev, Usp. Fiz. Nauk **109**, 91 (1973) [Sov. Phys Usp. **16**, 31 (1973)].

[27] K. K. Gudima, G. A. Ososkov, and V. D. Toneev, Yad. Fiz. **21**, 260 (1975) [Sov. J. Nucl. Phys. **21**, 138 (1975)].

[28] S. G. Mashnik and V. D. Toneev, MODEX—the Program for Calculation of the Energy Spectra of Particles Emitted in the Reactions of Pre-Equilibrium and Equilibrium Statistical Decays, JINR Communication P4-8417, Dubna, USSR, 1974 (unpublished); https://mcnp.lanl.gov/

[29] N. S. Amelin, K. K. Gudima, and V. D. Toneev, Yad. Fiz. **51**, 512 (1990) [Sov. J. Nucl. Phys. **51**, 327 (1990)]; Yad. Fiz. **51**, 327 (1990) [Sov. J. Nucl. Phys. **51**, 272 (1990)].

[30] I. Pshenichnov, A. Botvina, I. Mishustin, and W. Greiner, Nucl. Instrum. Methods B **268**, 604 (2010).

[31] D. Hansen, A. Lühr, N. Sobolevsky, and N. Bassler, Phys. Med. Biol. **57**, 2393 (2012); M. Hultqvist, M. Lazzeroni, A. Botvina, I. Gudowska, N. Sobolevsky, and A. Brahme, *ibid.* **57**, 4369 (2012); A. Lühr, D. Hansen, R. Teiwes, N. Sobolevsky, O. Jakel, and N. Bassler, *ibid.* **57**, 5169 (2012).

[32] T. Ogawa, T. Sato, S. Hashimoto, and K. Niita, Nucl. Instrum. Methods A **723**, 36 (2013); T. Sato, K. Niita, N. Matsuda, S. Hashimoto, Y. Iwamoto, S. Noda, T. Ogawa, H. Iwase, H. Nakashima, T. Fukahori, K. Okumura, T. Kai, S. Chiba, T. Furuta, and L. Sihver, J. Nucl. Sci. Technol. **50**, 913 (2013).

[33] S. G. Mashnik and L. M. Kerby, Nucl. Instrum. Methods A **764**, 59 (2014).

[34] L. M. Kerby and S. G. Mashnik, Nucl. Instrum. Methods B **356-357**, 135 (2015).

[35] S. G. Mashnik, A. J. Sierk, K. A. Van Riper, and W. B. Wilson, Production and Validation of Isotope Production Cross Section Libraries for Neutrons and Protons to 1.7 GeV, LANL Report No. LA-UR-98-6000, Los Alamos, 1998; in *Proceedings of the Fourth International Workshop on Simulating Accelerator Radiation Environments (SARE-4)*, Knoxville, TN, USA, September 13–16, 1998, edited by T. A. Gabriel (ORNL, Oak Ridge, USA, 1999), pp. 151–162.

[36] R. E. L. Green, R. G. Korteling, J. M. D'Auria, K. P. Jackson, and R. L. Helmer, Phys. Rev. C **35**, 1341 (1987).

[37] J. Benecke, T. Chou, C. Yang, and E. Yen, Phys. Rev. **188**, 2159 (1969).

[38] M. Fidelus, Ph.D. thesis, Cracow University, Poland, 2010 (unpublished).

[39] L. M. Kerby, Ph.D. thesis, University of Idaho, 2015 (unpublished).

[40] L. M. Kerby, S. G. Mashnik, K. K. Gudima, A. J. Sierk, J. S. Bull, and M. R. James, Production of Energetic Heavy Clusters in CEM and MCNP6, LANL Report LA-UR-15-29524, Los Alamos, 2015.

[41] A. Y. Konobeyev and U. Fischer, Status of Evaluation of ^{9}Be DPA and Gas Production Cross-Sections at Neutron Incident Energies up to 200 MeV, presentation at the Fall 2014 Nuclear Data Week, 24–28 November 2014, NEA, Issy-le-Moulineaux, France, http://www.oecdnea.org/dbdata/meetings/nov2014/; Evaluation of Atomic Displacement and Gas Production Cross-Section for ^{9}Be Irradiated with Neutrons at Energies up to 200 MeV, Institut für Neutronenphysik und Reaktortechnik, Karlsruher Institut für Technologie (KIT) technical report, 2015.

[42] A. R. Junghans, M. de Jong, H.-G. Clerc, A. V. Ignatyuk, G. A. Kudyaev, and K.-H. Schmidt, Nucl. Phys. A **629**, 635 (1998); J.-J. Gaimard and K.-H. Schmidt, *ibid.* **531**, 709 (1991).

[43] A. Koning, S. Hilaire, and M. Duijvestijn, in *Proceedings of the Internationla Conference on Nuclear Data for Science & Technology (ND2004)*, September 26–October 1, 2004, Santa Fe, edited by R. Haight, M. Chadwick, T. Kawano, and P. Talou, AIP Conf. Proc. No. 769 (AIP, New York, 2005), p. 1154; http://www.talys.eu/

[44] M. Meier, W. Amian, C. Goulding, G. Morgan, and C. Moss, Nucl. Sci. Eng. **110**, 289 (1992).

[45] M. Meier, D. Clark, C. Goulding, J. McClelland, G. Morgan, C. Moss, and W. Mian, Nucl. Sci. Eng. **102**, 310 (1989).

[46] T. Ericson, Adv. Phys. **9**, 425 (1960).

[47] F. C. Williams, Jr., Phys. Lett. B **31**, 184 (1970).

[48] F. C. Williams, Jr., Nucl. Phys. A **166**, 231 (1971).

[49] I. Ribansky, P. Oblozinsky, and E. Betak, Nucl. Phys. A **205**, 545 (1973).

[50] G. Mantzouranis, H. A. Weidenmüller, and D. Agassi, Z. Phys. A **276**, 145 (1976).

[51] C. Kalbach, Phys. Rev. C **37**, 2350 (1988).

[52] D. B. Pelowitz, J. W. Durkee, J. S. Elson, M. L. Fensin, J. S. Hendricks, M. R. James, R. C. Johns, G. W. McKinney, S. G. Mashnik, J. M. Verbeke, L. S. Waters, and T. A. Wilcox, MCNPX 2.7.0 Extensions, LANL Report LA-UR-11-02295, Los Alamos, 2011 and refrences therein; https://mcnpx.lanl.gov/

[53] N. V. Mokhov, K. K. Gudima, C. C. James, M. A. Kostin, S. G. Mashnik, E. Ng, J.-F. Ostiguy, I. L. Rakhno, A. J. Sierk, and S. I. Striganov, Rad. Prot. Dosim. **116**, 99 (2005); http://www-ap.fnal.gov/MARS/

[54] I. Dostrovsky, Z. Frankel, and G. Friedlander, Phys. Rev. **116**, 683 (1959); I. Dostrovsky, P. Rabinowitz, and R. Bivins, *ibid.* **111**, 1659 (1958).

[55] R. Tripathi, F. Cucinotta, and J. Wilson, Nucl. Instrum. Methods B **117**, 347 (1996); **129**, 11 (1997); **155**, 349 (1999).

[56] V. S. Barashenkov and A. Polanski, Electronic Guide for Nuclear Cross-Sections, JINR Communication E2-94-417, JINR, Dubna, Russia, 1994.

[57] C. Kalbach, J. Phys. G **24**, 847 (1998).

[58] H. H. K. Tsang, G. R. Srinivasan, and N. Azziz, Phys. Rev. C **42**, 1598 (1990).

[59] S. G. Mashnik, R. E. Prael, and K. K. Gudima, Implementation of CEM03.01 into MCNP6 and its Verification and Validation Running through MCNP6. CEM03.02 Upgrade, LANL Report LA-UR-06-8652, Los Alamos, 2007; https://mcnp.lanl.gov/

[60] R. Prael, A. Ferrari, R. Tripathi, and A. Polanski, in *Porceedings of the Fourth International Workshop on Simulating Accelerator Radiation Environments (SARE-4)*, Knoxville, TN, USA, September 13–16, 1998, edited by T. A. Gabriel (ORNL, Oak Ridge, USA, 1999), pp. 171–181.

[61] L. M. Kerby and S. G. Mashnik, LANL Fiscal Year 2014 Report, LANL Report LA-UR-14-27533, Los Alamos, 2014; http://www.osti.gov/scitech/biblio/1162152

[62] R. Carlson, At. Data Nucl. Data Tables **63**, 93 (1996).

[63] V. S. Barashenkov, *Cross Sections of Interaction of Particles and Nuclei with Nuclei* (JINR, Dubna, Russia, 1993); M. Mazarakis and W. Stephens, Phys. Rev. C **7**, 1280 (1973); M. Takechi *et al.*, *ibid.* **79**, 061601 (2009).

[64] A. N. Golovchenko, J. Skvarc, N. Yasuda, M. Giacomelli, S. P. Tretyakova, R. Ilic, R. Bimbot, M. Toulemonde, and T. Murakami, Phys. Rev. C **66**, 014609 (2002); C. Zeitlin, S. Guetersloh, L. Heilbronn, J. Miller, A. Fukumura, Y. Iwata, and T. Murakami, *ibid.* **76**, 014911 (2007).

[65] J. R. Wu and C. C. Chang, Phys. Rev. C **17**, 1540 (1978).

[66] E. Betak, Acta Phys. Slovaca **26**, 21 (1976).

[67] V. Blideanu, F. R. Lecolley, J. F. Lecolley, T. Lefort, N. Marie, A. Atac, G. Ban, B. Bergenwall, J. Blomgren, S. Dangtip, K. Elmgren, P. Eudes, Y. Foucher, A. Guertin, F. Haddad, A. Hildebrand, C. Johansson, O. Jonsson, M. Kerveno, T. Kirchner, J. Klug, C. Brun, C. Lebrun, M. Louvel, P. Nadel-Turonski, L. Nilsson, N. Olsson, S. Pomp, A. V. Prokofiev, P.-U. Renberg, G. Riviere, I. Slypen, L. Stuttge, U. Tippawan, and M. Osterlund, Phys. Rev. C **70**, 014607 (2004).

[68] W. Press, W. Vetterling, S. Teukolsky, and B. Flannery, *Numerical Recipes in C: The Art of Scientic Computing* (Cambridge University Press, Cambridge, 1992).

[69] V. D. Toneev and K. K. Gudima, Nucl. Phys. A **400**, 173c (1983).

[70] K. K. Gudima, G. Röpke, H. Schulz, and V. D. Toneev, The Coalescence Model and Pauli Quenching in High-Energy Heavy-Ion Collisions, JINR Preprint JINR-E2-83-101, Dubna, 1983; H. Schulz, G. Röpke, K. K. Gudima, and V. D. Toneev, Phys. Lett. B **124**, 458 (1983).

[71] L. M. Kerby and S. G. Mashnik, An Expanded Coalescence Model within the Intranuclear Cascade of CEM, LANL Report LA-UR-15-20322, Los Alamos, 2015.

[72] R. E. L. Green, R. G. Korteling, and K. P. Jackson, Phys. Rev. C **29**, 1806 (1984).

[73] K. K. Gudima and S. G. Mashnik, *Proceedings of the 11th International Conference on Nuclear Reaction Mechanisms*, Varenna, Italy, June 12–16, 2006, edited by E. Gadioli (Univ. Milan, 2006), pp. 525–534.

[74] N. S. Amelin, Simulation of Nuclear Collisions at High Energy in the Framework of the Quark-Gluon String Model, JINR Communication JINR-86-802, Dubna, 1986; A. B. Kaidalov, Yad. Fiz. **45**, 1452 (1987) [Sov. J. Nucl. Phys. **45**, 902 (1987)].

[75] M. Mocko, Ph.D. thesis, Michigan State University, 2006 (unpublished); M. Mocko, M. B. Tsang, L. Andronenko, M. Andronenko, F. Delaunay, M. Famiano, T. Ginter, V. Henzl, D. Henzlova, H. Hua, S. Lukyanov, W. G. Lynch, A. M. Rogers, M. Steiner, A. Stolz, O. Tarasov, M.-J. van Goethem, G. Verde, W. S. Wallace, and A. Zalessov, Phys. Rev. C **74**, 054612 (2006).

[76] L. Heilbronn, C. Zeitlin, Y. Iwata, T. Murakami, H. Iwase, T. Nakamura, T. Nunomiya, H. Sato, H. Yashima, R. M. Ronningen, and K. Ieki, Nucl. Sci. Eng. **157**, 142 (2007); T. Nakamura and L. Heilbronn, *Handbook on Secondary Particle Production and Transport by High-Energy Heavy Ions* (World Scientic, Singapore, 2006).

[77] S. Frankel, W. Frati, M. Gazzaly, Y. D. Bayukov, V. I. Efremenko, G. A. Leksin, N. A. Nikiforov, V. I. Tchistilin, Y. M. Zaitsev, and C. F. Perdrisat, Phys. Rev. C **20**, 2257 (1979).

[78] B. V. Jacak, G. D. Westfall, G. M. Crawley, D. Fox, C. K. Gelbke, and L. H. Harwood, *et al.*, Phys. Rev. C **35**, 1751 (1987).

[79] M. Toppi *et al.*, Phys. Rev. C **93**, 064601 (2016).

[80] M.-C. Lemaire, S. Nagamiya, O. Chamberlain, G. Shapiro, S. Schnetzer, H. Steiner, and I. Tanihata, Tables of Light-Fragment Inclusive Cross Sections in Relativistic Heavy Ion Collisions. Part I. C + C, C + Pb, Ne + NaF, Ne + Cu, Ne + Pb $\rightarrow \pi^{\pm}, p, d, t, {}^{3}\mathrm{He}$; $E_{\mathrm{BEAM}} = 800$ MeV/A, Lawrence Berkeley National Laboratory Report LBL-8463 (unpublished), 1978; S. Nagamiya, M.-C. Lemaire, E. Moeller, S. Schnetzer, G. Shapiro, H. Steiner, and I. Tanihata, Phys. Rev. C **24**, 971 (1981).

[81] J. Franz, P. Koncz, E. Roessle, C. Sauerwein, H. Schmitt, K. Schmoll, J. Eroe, Z. Fodor, J. Kecskemeti, Z. Kovacs, and Z. Seres, Nucl. Phys. A **510**, 774 (1990).

[82] R. A. Schumacher, G. S. Adams, D. R. Ingham, J. L. Matthews, W. W. Sapp, R. S. Turley, R. O. Owens, and B. L. Roberts, Phys. Rev. C **25**, 2269 (1982).

[83] T. Nakamoto, K. Ishibashi, N. Matsufuji, N. Shigyo, K. Maehata, H. Arima, S. Meigo, H. Takada, S. Chiba, and M. Numajiri, J. Nucl. Sci. Technol. **34**, 860 (1997).

[84] J. Benlliure, P. Armbruster, M. Bernas, A. Boudard, J. Dufour, T. Enqvist, R. Legrain, S. Leray, B. Mustapha, F. Rejmund, K.-H. Schmidt, C. Stephan, L. Tasaan-Got, and C. Volant, Nucl. Phys. A **683**, 513 (2001); F. Rejmund, B. Mustapha, P. Armbruster, J. Benlliure, M. Bernas, A. Boudard, J. Dufour, T. Enqvist, R. Legrain, S. Leray, K.-H. Schmidt, C. Stephan, J. Taieb, L. Tassan-Got, and C. Volant, *ibid.* **683**, 540 (2001).

[85] A. Fomichev, V. Dushin, S. Soloviev, A. Fomichev, and S. Mashnik, Neutron Induced Fission Cross Sections for ^{240}Pu, ^{243}Am, ^{209}Bi, ^{nat}W Measured Relative to ^{235}U in the Energy Range 1–350 MeV, V. G. Khlopin Radium Institute Preprint RI-262, St. Petersburg, Russia, 2004; LANL Report LA-UR-05-1533, Los Alamos, 2005; https://mcnp.lanl.gov/

[86] D. Tarrío *et al.* (n_TOF Collaboration), Phys. Rev. C **83**, 044620 (2011).

[87] R. Prael, Tally Edits for the MCNP6 GENXS Option, LANL Report LA-UR-11-02146, Los Alamos, 2011.

[88] L. M. Kerby, S. G. Mashnik, and J. S. Bull, GENXS Expansion to Include Fragment Spectra of Heavy Ions, LANL Report LA-UR-15-24006, Los Alamos, 2015); http://www.osti.gov/scitech/biblio/1183395/